remote sensing

MDPI

Article

Spatiotemporal Patterns and Morphological Characteristics of *Ulva prolifera* Distribution in the Yellow Sea, China in 2016–2018

Yingzhi Cao [1], Yichen Wu [2,*], Zhixiang Fang [2], Xiaojian Cui [1], Jianfeng Liang [1] and Xiao Song [1]

[1] National Marine Data and Information Service, Tianjin 300171, China; caoyingzhi@nmdis.org.cn (Y.C.); cuixiaojian@nmdis.org.cn (X.C.); liangjianfeng@nmdis.org.cn (J.L.); songxiao@nmdis.org.cn (X.S.)

[2] State Key Laboratory of Information Engineering in Surveying, Mapping and Remote Sensing, Wuhan University, Wuhan 430079, China; zxfang@whu.edu.cn

* Correspondence: yichenwu@whu.edu.cn; Tel.: +86-27-68779889

Received: 22 December 2018; Accepted: 14 February 2019; Published: 21 February 2019

Abstract: The world's largest macroalgal blooms, *Ulva prolifera*, have appeared in the Yellow Sea every summer on different scales since 2007, causing great harm to the regional marine economy. In this study, the Normalized Difference of Vegetation Index (NDVI) index was used to extract the green tide of *Ulva prolifera* from MODIS images in the Yellow Sea in 2016–2018, to investigate its spatiotemporal patterns and to calculate its occurrence probability. Using the standard deviational ellipse (SDE), the morphological characteristics of the green tide, including directionality and regularity, were analyzed. The results showed that the largest distribution and coverage areas occurred in 2016, with 57,384 km^2 and 2906 km^2, respectively and that the total affected region during three years was 163,162 km^2. The green tide drifted northward and died out near Qingdao, Shandong Province, which was found to be a high-risk region. The coast of Jiangsu Province was believed to be the source of *Ulva prolifera*, but it was probably not the only one. The regularity of the boundary shape of the distribution showed a change that was opposite to the variation of scale. Several sharp increases were found in the parameters of the SDE in all three years. In conclusion, the overall situation of *Ulva prolifera* was still severe in recent years, and the sea area near Qingdao became the worst hit area of the green tide event. It was also shown that the sea surface wind played an important part in its migration and morphological changes.

Keywords: *Ulva prolifera*; green tide; MODIS; spatiotemporal patterns; morphological characteristics

1. Introduction

In 2007, a small-scale green tide formed by *Ulva prolifera* was observed for the first time in the coastal area of Qingdao, China [1]. However, the free-floating macroalgae appeared again during the Olympic Games in 2008, covering approximately 13,000–30,000 km^2 and posing a great threat to the Olympic sailing competition [2]. With intensive efforts, over 16,000 people and 600 boats were organized to clean up the coastal water for sailing training, resulting in substantial economic losses [2–5]. Since then, the world's largest macroalgal bloom has become a continuous phenomenon in the southern waters of the Yellow Sea, and it has attracted great attention for marine researchers. Also, *Ulva prolifera* has been confirmed as the only dominant species in the Yellow Sea green tides, by both morphology and molecular analyses [6–8].

Because of the sudden outbreak of green tide and its migration along with the wind direction and tide, it is difficult to meet the needs for disaster prevention and mitigation by the traditional sampling method of ship surveys. Remote sensing (RS) technology has the advantage of fast data acquisition, large coverage, and dynamic monitoring. It can monitor the origin, spatial distribution,

dynamic process, scale, and migration of green tides in real time. It has become one of the irreplaceable means for green tide monitoring and early warning. A mass of past studies have documented the appearance, statistics, and causes of *U. prolifera* through RS.

Using satellite tracking methods, the world's largest green tide in the Yellow Sea was reported to grow every year in late spring, with a peak in June, and finally to disappear in August [1,2,9–11]. Most researchers believe that Subei Shoal serves as the "cradle" of large-scale green tides, and this hypothesis was confirmed by previous studies [2,10,12,13]. Over the years, the maximum coverage and water distribution area during the bloom season were recorded to show the severity of *U. prolifera* [12,14,15], which varied in different years. On an annual scale, mean *Ulva* coverage decreased after 2008, but it increased rapidly after 2012 from 8 km^2 in 2012 to 116 km^2 in 2015 [11]. Meanwhile, the transport patterns of free-floating algae were numerically modeled and validated by satellite observations. Under wind-current action, the algae drifted from Jiangsu Province northward to the offshore region of Qingdao, Shandong Province [10,16], which has become the most severely affected area in recent years.

To explore the interannual variation of *U. prolifera*, researchers have used various remote-sensing images and various image recognition methods, but mostly from the viewpoint of the distribution range, coverage area, or migration trajectory. Images from the Moderate Resolution Imaging Spectroradiometer (MODIS) with a 250 m spatial resolution are the most popular, and were used by Liu et al. [2] to quantify the covered and affected areas of *U. prolifera*. Cui et al. [17] compared the imaging ability of multiple data sources, including MODIS, HJ-1A/B (China Small Satellite Constellation for Environment and Disaster Monitoring and Forecasting), charge-coupled devices (CCDs), Environmental Satellite (ENVISAT), and Advanced Synthetic Aperture Radar (ASAR) for macroalgae monitoring and drift velocity estimation. Using the Geostationary Ocean Color Imager (GOCI), Song et al. [18] tracked the pathway of floating green algae blooms. More recently, MODIS estimates were compared for the first time with concurrent high resolution (3 m) airborne synthetic aperture radar (SAR) data by Cui et al. [19], with the purpose of assessing and refining our knowledge of green macro-algal coverage.

The Normalized Difference of Vegetation Index (NDVI) may be the most commonly used index for detecting *U. prolifera* in sea areas [20]. Other indices, such as the Floating Algae Index (FAI), the Virtual Baseline Floating macroAlgae Height (VB-FAH), and the Difference of Vegetation Index (DVI), were found to be less sensitive to perturbations from sun glint and possibly from aerosols, but they were suitable for high-resolution images [21]. With the accelerating development of deep learning (DL), more and more DL-based methods are being applied to RS images. For example, an Elegant End-to-End Fully Convolutional Network (E3FCN) was proposed by Yin et al. [22] for green-tide coverage detection.

The distribution and coverage area statistics indicate the general situation of *U. prolifera* growth, which is beneficial for evaluating the severity of green tide events, while the migration of the barycenter plays an important part in prediction models of *U. prolifera*. In addition to the conventional aspects described above, this paper has concentrated on the spatial distribution of the occurrence probability of *U. prolifera* and the morphological characteristics of its distribution range by analyzing the growth situation in detail during 2016 to 2018. According to probabilities, the grade of severity of each event was classified in the study area, which generated a reliable basis for defining the safe area for offshore operations. Furthermore, two morphological evaluation targets, directionality and regularity, were considered. The exploration of directional laws provides a new method for discovering the factors that cause directional mutations in the distribution of *U. prolifera*, whereas regularity reflects the difficulty of governing such a distribution. By synthesizing the analysis of all the above indicators, the current situation and development trend of *U. prolifera* can be better characterized, which would be conducive to long-term monitoring, prevention and control, early warning, and the prediction of green tide events.

2. Materials and Methods

2.1. Study Area

Connected to the Bohai Sea in the north and to the East China Sea in the south, the Yellow Sea is a typical semi-enclosed epi-continental sea area in the northwestern Pacific Ocean [23]. The climate of the Yellow Sea is characterized by cold and dry winters and warm and humid summers. The annual variation of water temperature is 13–24 °C, and the salinity of seawater is 33‰ to 34‰, creating an excellent region for algal blooms. Given the distribution of *U. prolifera* for a number of years, the study area covered from 118°E to 125°E and from 31°N to 38°N in the southern Yellow Sea (Figure 1). This region contains the coastal areas of the Jiangsu and Shandong Provinces, which have experienced outbreaks of green algal blooms since 2007 [1].

Figure 1. Map of the study area and major cities along the coast.

2.2. Remote-Sensing Data

MODIS is an optical sensor on the satellite of the Earth Observation System (EOS). It contains 36 optical channels and realizes full spectral coverage ranging from 0.4 μm (visible light) to 14.4 μm (thermal infrared). The sun-synchronous near-polar orbit satellites Terra and Aqua carrying MODIS transit twice a day to achieve global observation every two days. The MODIS data have three resolutions: 1000 m, 500 m, and 250 m. Among these, the 250 m product covers red and near-infrared bands that can be used to discriminate clouds, plants, and land. These characteristics of the MODIS data are helpful for obtaining information about *U. prolifera* and monitoring its outbreaks over a large continuous area, as has been confirmed in previous studies [2,14].

The re-entry period of the MODIS images is one day, which is shorter than that of other high-resolution images. For example, the Landsat-8 re-entry period is 16 days, and that of HJ-1 CCD is 2 days. With the advantages of comprehensive time coverage and simple processing, MODIS is suitable for real-time, large-area monitoring of *U. prolifera*.

The data used in this study were all downloaded from the National Aeronautics and Space Administration (NASA) data sharing website [24]. MODIS Level-1B 250 m class data (MOD02QKM) and MODIS geolocation data (MOD03, Geographic Location File) were selected as data sources from May to August during 2018. MOD03 was involved in the geometric correction of MODIS02QKM.

2.3. Methods

Figure 2 illustrates the research flow of this study. All tasks were divided into four main parts, including remote-sensing image downloading, data preprocessing, *U. prolifera* extraction, and analysis of relevant patterns. Compared to Landsat-8 (30 m) and HJ-1 CCD (30 m), the spatial resolution of the MODIS data (250 m) used in this study was lower, and therefore the problem of mixed pixels was more serious than with the other images. Together with considerations of image time and various kinds of methodology, there was no ideal way to quantify the coverage of *U. prolifera* accurately, and selecting the threshold was also a tricky problem [25,26]. In this study, instead of exploring the improvement of different methods and the discrimination of mixed pixels, we focused on morphological changes in *U. prolifera*, to explore its development by identifying its patterns and trends. Moreover, algae floating on the sea are identified by remote sensing images, but the biomass of the algae below the sea surface is not involved in this paper.

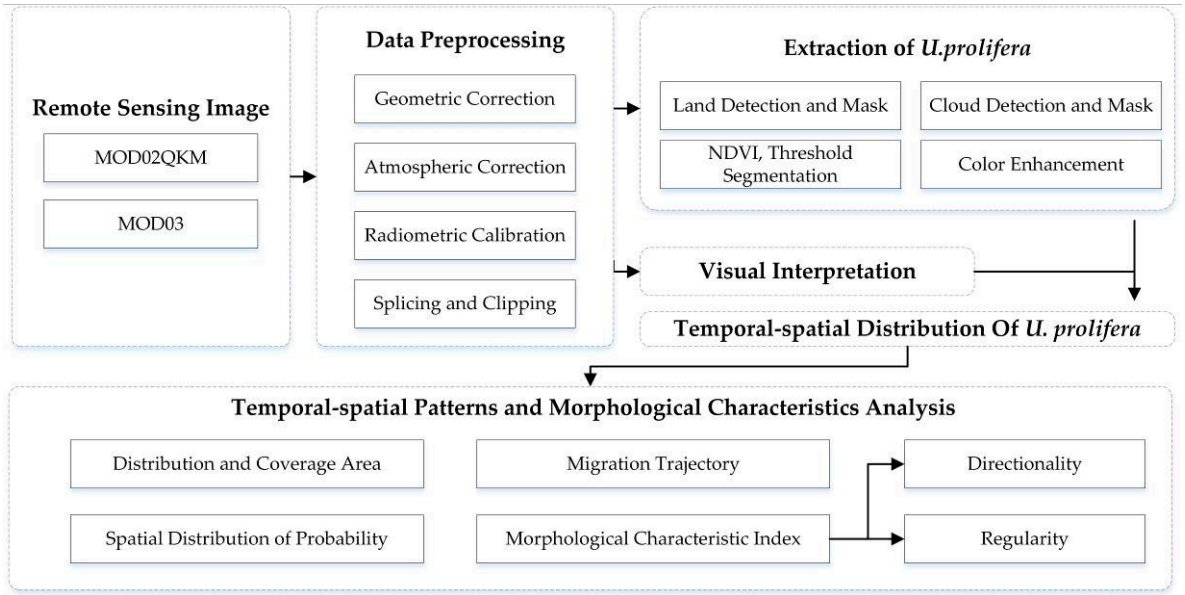

Figure 2. Research flow chart for this study.

2.3.1. Data Preprocessing and Extraction of *U. prolifera*

Similarly to land vegetation, *U. prolifera* has a reflection valley in the red wavelength, and a peak in the near-infrared. Based on the spectral reflectance differences of ground objects, the ratio operation can highlight the characteristics of vegetation in images, identify the plant category, and extract the green biomass of the plant. A series of indices based on these principles have been used to delineate *U. prolifera*; for example, the NDVI index [9,14,20], which is the best indicator of the growth state and coverage area of land vegetation, and which is widely used in vegetation remote sensing [27]. Compared with other parameters, such as FAI and VB-FAH, NDVI is more sensitive to perturbations from sun glint and possibly from aerosols, and the value is easily saturated, and the sensitivity to high vegetation density region is reduced. However, NDVI has a wide adaptability to different remote sensing images, which also can partially eliminate the influence of radiation changes that are related to atmospheric conditions such as solar altitude angle, satellite observation angle, terrain, and cloud shadow.

The distribution of *U. prolifera* can usually be expressed in two areal forms, the coverage area and the distribution area. The former is a collection of pixels of *U. prolifera* that can be directly identified in the remote-sensing images. Clustered pixels create patches with different shapes and sizes, which is also called the scattered fragments of *U. prolifera*. The distribution area, which can also be called the influence area, aggregates scattered fragments of the *U. prolifera* coverage area into relatively large fragmented areas, including all of the patches and the region among the adjacent patches.

In this study, the MODIS images were first preprocessed. Based on MOD03 data and the MODIS Swath Tool (MST) software, the geometric correction results of MOD02QKM data were obtained in batch form. Then, radiometric calibration, atmospheric correction, image splicing, and clipping, and band fusion of the remote-sensing images were carried out by the Environment for Visualizing Images (ENVI) using the Interactive Data Language (IDL). After sea-land separation and cloud masking, the distribution information of *U. prolifera* was obtained by calculating the NDVI, which was first applied by Rouse et al. [28] in the Great Plains study, and which can be calculated as:

$$NDVI = \frac{R_{NIR} - R_{RED}}{R_{NIR} + R_{RED}} \quad (1)$$

where R_{NIR} and R_{RED} represents the near-infrared and red bands, respectively.

The value of $NDVI$ is between -1 to 1, negative values indicate cloud, water, snow, and some other objects with highly reflecting to visible light; 0 means rock or bare soil, while NIR and R are approximately equal; a positive value indicates that there is vegetation coverage, which increases with the increase of coverage. The threshold selection is mainly based on these rules.

By combining gray segmentation with manual interpretation, the influence and coverage range of the green tide was determined. Then, the layer was transformed into vector data, and the ArcGIS software was used to calculate the area of the vectorial map patches. Finally, the temporal–spatial information describing the coverage area and the distribution margin of *U. prolifera* were obtained.

2.3.2. Spatial Probability Distribution

The spatial probability distribution is the frequency of occurrence of *U. prolifera* in a certain spatial position at a specific time. A larger value represents a greater probability of a green tide event during a period of time in the study area. In this experiment, a series of images were selected, with good weather conditions and equal intervals as far as possible, as the research objects were used in the probability calculations. The spatial probability distribution can be calculated as:

$$P = \frac{D_1}{D_0} \quad (2)$$

where D_1 represents the number of times that *U. prolifera* appeared in a specific spatial position, and D_0 is the total number of statistical intervals.

2.3.3. Migration Trajectory of the Barycenter

The concept of the center of gravity in physics and the theory of spatial statistics were combined to study the drift path of *U. prolifera*. The coverage area of *U. prolifera* was regarded as a set of geometric blocks with uniform mass, and the center of gravity was the concentration point of its drift stress. Based on the principle described above, using ArcGIS as a technology platform, data processing was divided into six steps (Figure 3).

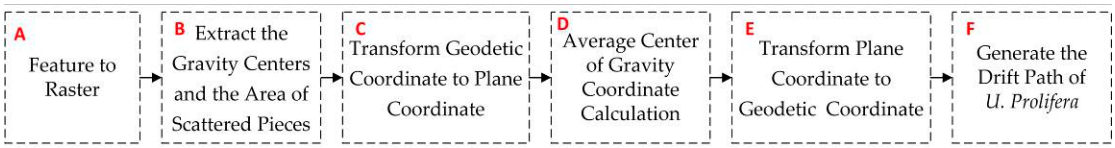

Figure 3. Data processing steps.

Among these steps, using the spatial average method to calculate the center of gravity was the most critical. Suppose that the coverage area of *U. prolifera* on a certain day consists of n units P;

the barycentric coordinates of the i-th unit are (x_i,y_i), the unit area is m_i, and the center of gravity is denoted as $Q(\overline{x}, \overline{y})$:

$$\begin{cases} \overline{x} = \sum_{i=1}^{n} x_i m_i / \sum_{i=1}^{n} m_i \\ \overline{y} = \sum_{i=1}^{n} y_i m_i / \sum_{i=1}^{n} m_i \end{cases} \quad (3)$$

2.3.4. Morphological Characteristic Index

This paper evaluated the morphological distribution characteristics of *U. prolifera* from the two viewpoints of directionality and regularity. The directional features represented development trends that were related to directional factors such as ocean current and wind, whereas the regularity were used to evaluate the degree of convergence.

The standard deviational ellipse (SDE) was proposed by Lefever [29], taking the center, x-axis, y-axis, and azimuth angle as the parameters. The SDE is a method of spatial statistics that quantitatively describes the characteristics of the spatial distribution of geographical factors. The calculation of SDE was performed using ArcGIS software. To show the directionality of the distribution of *U. prolifera*, two SDE parameters, oblateness, and direction angle, were used in this study. The oblateness is a value that is between 0 and 1, and it represents the difference between the long and short axes of the ellipse. The closer the value is to 1, the more significant the directionality. The direction angle is the angle between the positive North direction (clockwise direction) and the long axis of the ellipse. The key formula is:

$$tan\,\theta = \frac{\left(\sum_{i=1}^{n} \tilde{x}_i^2 - \sum_{i=1}^{n} \tilde{y}_i^2\right) + \sqrt{\left(\sum_{i=1}^{n} \tilde{x}_i^2 - \sum_{i=1}^{n} \tilde{y}_i^2\right)^2 + 4\left(\sum_{i=1}^{n} \tilde{x}_i \tilde{y}_i\right)^2}}{2\sum_{i=1}^{n} \tilde{x}_i \tilde{y}_i} \quad (4)$$

$$\begin{aligned} \sigma_x &= \sqrt{2}\sqrt{\frac{\sum_{i=1}^{n} (\tilde{x}_i \cos\theta - \tilde{y}_i \sin\theta)^2}{n}} \\ \sigma_y &= \sqrt{2}\sqrt{\frac{\sum_{i=0}^{n} (\tilde{x}_i \cos\theta + \tilde{y}_i \sin\theta)^2}{n}} \end{aligned} \quad (5)$$

$$e = \frac{a - b}{a} \quad (6)$$

where (x_i, y_i) represents the spatial location of the objects; $(\tilde{x}_i, \tilde{y}_i)$ is the coordinate deviation from the location to the mean coordinate; σ_x, σ_y represent the standard deviation on the x- and y-axes respectively; θ is the direction angle; e is the oblateness; and a, b represent the length of the long and short axes of the ellipse.

The second characteristic is regularity. It is known that under the condition of equal area, the longer the perimeter, the more irregular the shape boundary. This study uses the ratio between perimeter and area (R) to indicate the difference in the perimeter per unit area, which is calculated as:

$$R = \frac{P}{A} \quad (7)$$

where P, A represent the perimeter and area of the distribution range of *U. prolifera*, respectively.

3. Results

3.1. Distribution and Coverage Area of U. prolifera

By synthesizing the observation conditions and taking into account the calculation of the distribution probability of *U. prolifera* in the later stage, 10 groups of relatively ideal results in 2018 with as equal time intervals as possible were obtained by screening (Figure 4); nine groups of results in 2017 and 2016 were shown in Figures 5 and 6, respectively.

In 2018, due to continuous thick cloud cover, the MODIS images of the Yellow Sea region in May were deleted during the screening stage. Therefore, the earliest time and place of *U. prolifera* could

not be accurately determined by interpretation of the MODIS images. The growth of *U. prolifera* had begun to take shape on June 3, when it was detected for the first time (Figure 4a). The distribution and coverage area were about 17,788 and 365 km^2 respectively. The maximum distribution and coverage area of *U. prolifera* occurred on June 24, 2018, with a distribution area of 33,502 km^2 and a coverage area of 2301 km^2 (Figure 4d). The growth of *U. prolifera* began on the coast of Jiangsu Province, gradually drifted northward, and finally disappeared near the coast of Qingdao. The change in the coverage area of *U. prolifera* was divided into four stages with the passage of time: a slow growth period, an eruption period, a stable period, and a rapid extinction period. From early to mid-June, the growth rate of *U. prolifera* was slow. The outbreak began in mid- to late June. Compared with the beginning of June, the distribution area was about twice as large, and the coverage area was about seven times as large. From late June to late July, *U. prolifera* entered a stable state. Its distribution area gradually decreased, but its coverage area stabilized at 800 to 900 km^2. In early August, *U. prolifera* entered a period of rapid extinction. The distribution and the coverage area decreased rapidly, and the algae disappeared completely from mid- to late August.

Compared with 2018, the temporal and spatial characteristics of the *U. prolifera* distribution in 2017 were quite different. At the end of April 2017, a large area of *U. prolifera* was found in the southeast corner of the Yellow Sea, with a distribution area of 18,643 km^2 and a coverage area of 841 km^2 (Figure 5a). In May, the *U. prolifera* gradually drifted northwest, and the distribution reached a maximum of 42261 km^2 on May 18 (Figure 5c). In mid–late May, *U. prolifera* appeared in the sea water near Jiangsu Province, and its scale expanded gradually. The *U. prolifera* in the southern part of the Yellow Sea disappeared quickly in June, and the large-scale outbreak of *U. prolifera* in the sea region near Shandong Province reached a maximum of 1871 km^2 on June 14 (Figure 5f). Since then, *U. prolifera* has decreased rapidly and died out near Qingdao in mid-July. In 2017, two outbreaks of *U. prolifera* in different locations were found, with a time-span of about one month.

U. prolifera initially appeared in 2016 at around mid-May, located near Jiangsu Province, which was similar to that in 2018. The initial distribution area and the coverage area of *U. prolifera* were 6952 km^2 and 381 km^2, respectively (Figure 6a). The growth of *U. prolifera* was slow in late May. From the beginning of June to the end of June, *U. prolifera* broke out on a large scale, with the maximum distribution area and coverage area reaching 57,384 km^2 and 2906 km^2 on June 25 (Figure 5e). In July, on a decreasing scale, the distribution of *U. prolifera* was continuously close to the coastline of Shandong Province scale, and died out near Qingdao at the end of July.

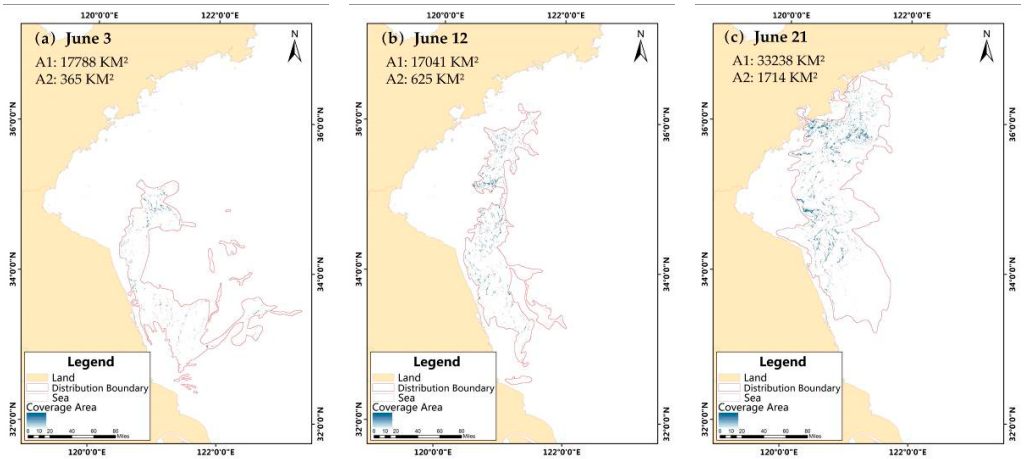

Figure 4. *Cont.*

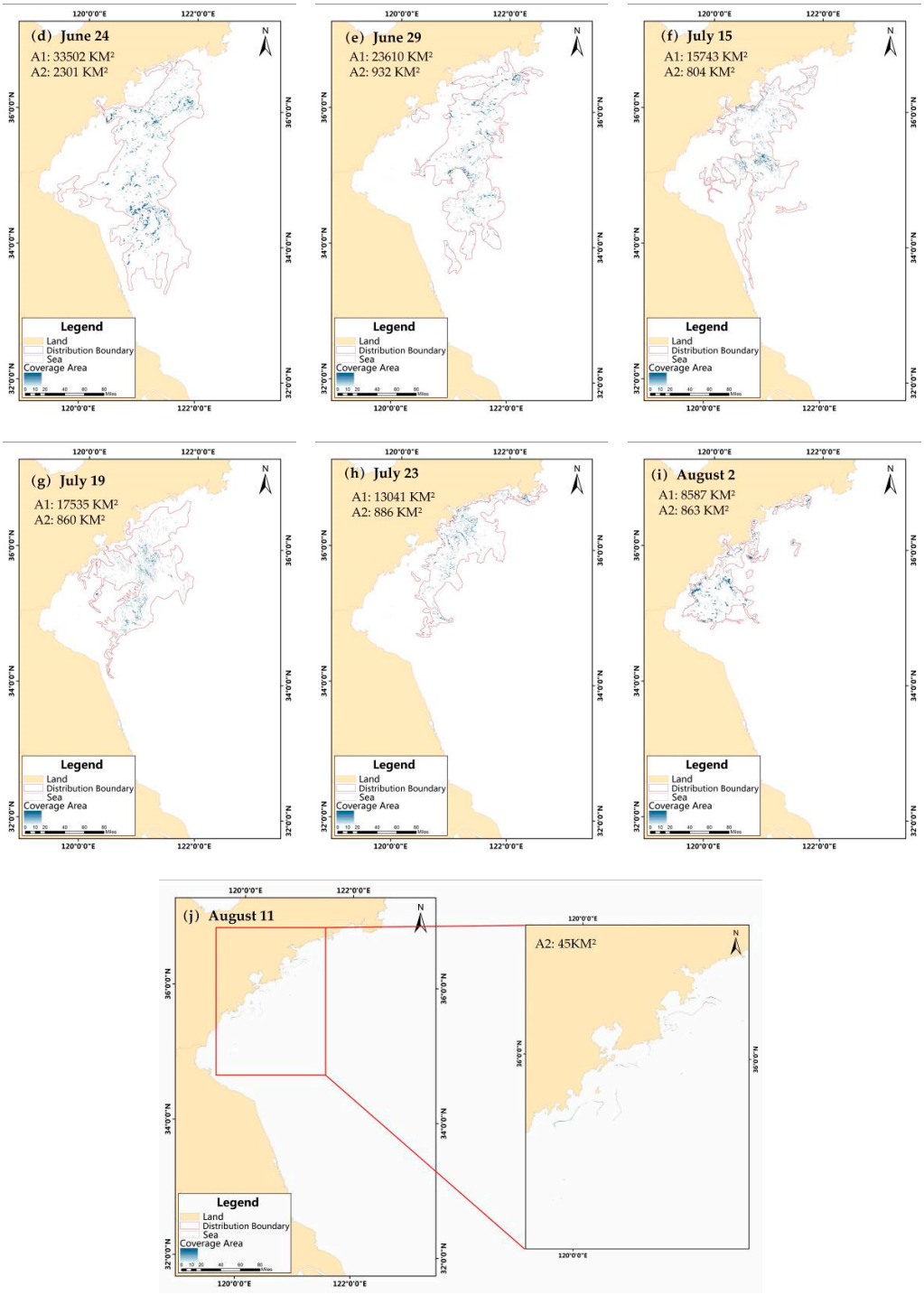

Figure 4. Spatial and temporal distribution of *U. prolifera* in the Yellow Sea, China in 2018. The area within the red line represents the distribution of *U. prolifera*. The blue gradient band represents the coverage area of *U. prolifera*, and the darker the color, the denser the algae are. The statistical values of the two kinds of areas appear in the upper left corner of each sub-figure; A1 denotes the affected area, and A2 represents the coverage area. (**a**) The situation of *U. prolifera* on June 3. (**b**) The situation of *U. prolifera* on June 12. (**c**) The situation of *U. prolifera* on June 21. (**d**) The situation of *U. prolifera* on June 24. (**e**) The situation of *U. prolifera* on June 29. (**f**) The situation of *U. prolifera* on July 15. (**g**) The situation of *U. prolifera* on July 19. (**h**) The situation of *U. prolifera* on July 23. (**i**) The situation of *U. prolifera* on August 2. (**j**) The situation of *U. prolifera* on August 11. In image (**j**), *U. prolifera* exists as only a slender filament, which has a negligible effect on the larger area. Therefore, only its coverage is counted. (Coordinate system: WGS_1984_UTM_zone_51N).

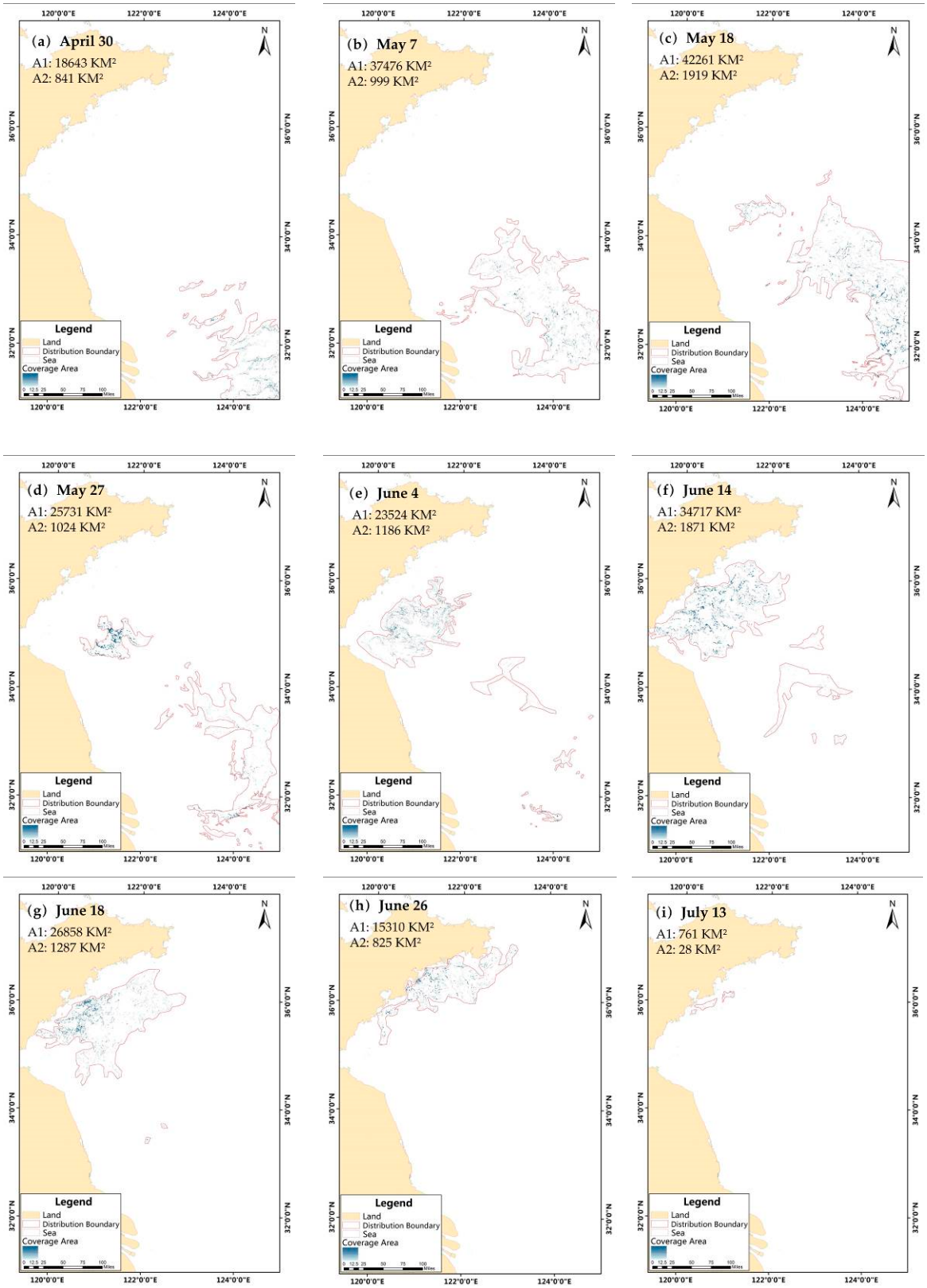

Figure 5. Spatial and temporal distribution of *U. prolifera* in the Yellow Sea, China in 2017. (**a**) The situation of *U. prolifera* on April 30. (**b**) The situation of *U. prolifera* on May 7. (**c**) The situation of *U. prolifera* on May 18. (**d**) The situation of *U. prolifera* on May 27. (**e**) The situation of *U. prolifera* on June 4. (**f**) The situation of *U. prolifera* on June 14. (**g**) The situation of *U. prolifera* on June 18. (**h**) The situation of *U. prolifera* on June 26. (**i**) The situation of *U. prolifera* on July 13.

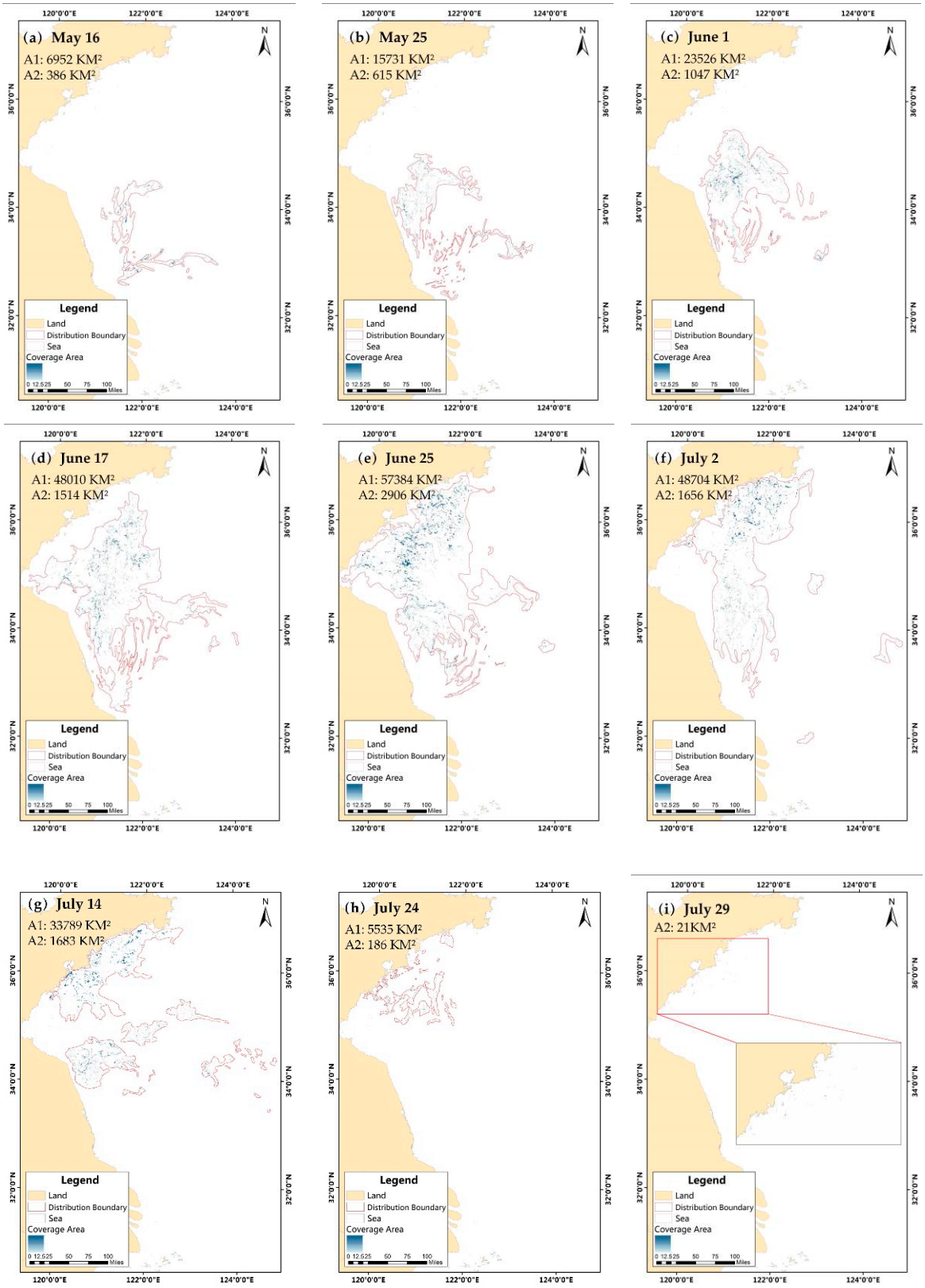

Figure 6. Spatial and temporal distribution of *U. prolifera* in the Yellow Sea, China in 2016. (**a**) The situation of *U. prolifera* on May 16. (**b**) The situation of *U. prolifera* on May 25. (**c**) The situation of *U. prolifera* on June 1. (**d**) The situation of *U. prolifera* on June 17. (**e**) The situation of *U. prolifera* on June 25. (**f**) The situation of *U. prolifera* on July 2. (**g**) The situation of *U. prolifera* on July 14. (**h**) The situation of *U. prolifera* on July 24. (**i**) The situation of *U. prolifera* on July 29. In image (**i**), only the coverage area of *U. prolifera* was counted, which existed as only a slender filament. The region in the red box is the coverage of *U. prolifera*, which is magnified in the detail image below.

3.2. Spatial Probability Distribution

The probability distribution of the occurrence of *U. prolifera* in the Yellow Sea during summer 2016–2018 was obtained by overlaying the distribution area (Figure 7). Each region can be classified according to its probability.

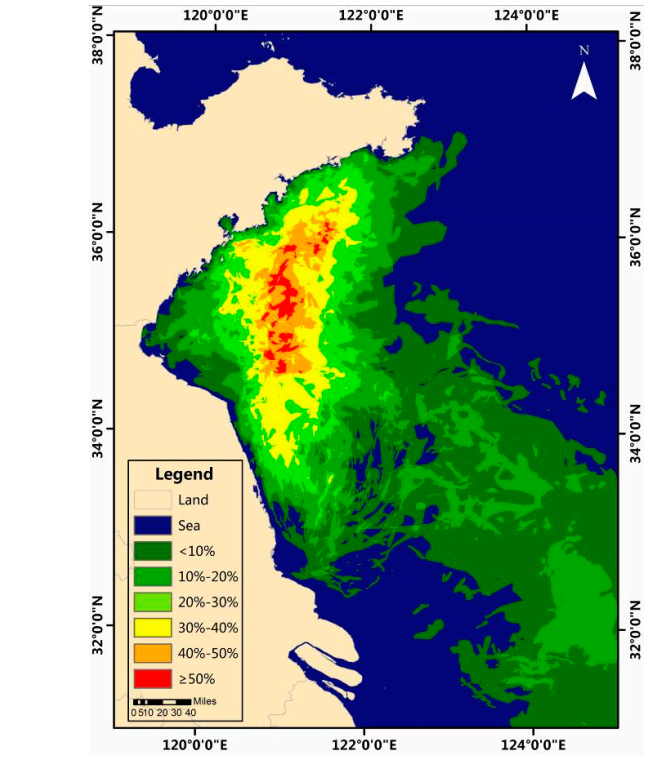

(**a**)

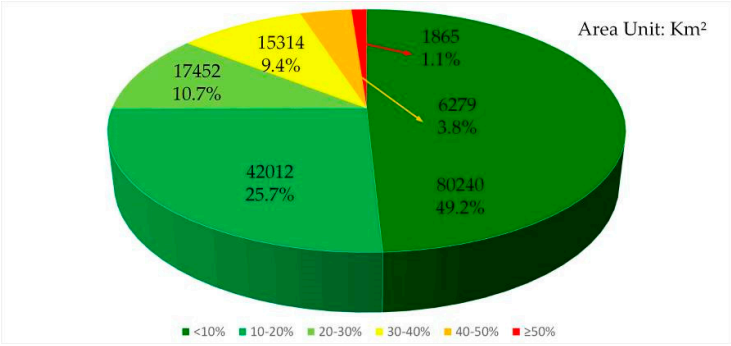

(**b**)

Figure 7. (**a**) The probability distribution of the occurrence of *U. prolifera* in the Yellow Sea during 2016–2018. From dark green to bright red, different colors represent different ranges of probability, with red ■ representing the highest-incidence area of *U. prolifera*. (**b**) The pie chart shows the percentage of the region corresponding to each probability as a part of the total affected area. The percentage and the specific area are shown on the pie chart. At the bottom of the pie chart, there is a probabilistic color bar. Each color corresponds to an interval of the probability of the occurrence of *U. prolifera*, the same as in (**a**).

In this study, a rating based on 10% intervals was used, and the area where the probability was greater than 50% was called the high risk area. Figure 7a shows the grading results. The probability distribution of *U. prolifera* showed an obvious central radiating trend, concentrated on the coast of Qingdao and its adjacent waters.

In the study area, the total influence range was about 163,162 km^2. The area and percentage of each probability class are shown in the pie chart in Figure 7b. Among these classes, the least probability (<10%) of occurrence accounted for 49.2% of the total area, and it was the most prevalent. In contrast, the high-risk area accounted for a small percentage of only 1.1%, which was only a small part of the total area. To a certain extent, the higher the probability, the smaller it's the percentage of the total area.

3.3. Drift Path of the Gravity Center

On the whole, the barycenter point gradually moved northward, and the main direction in 2016–2018 was 30° north by west, 35° north by west, and 16° north by east, respectively (Figure 8), with a high consistency between 2016 and 2017. From the perspective of the starting and ending points of the trajectories of these three years, which showed that *U. prolifera* originally grew off the southeast Yellow Sea and died out near Qingdao, Shandong Province, there was a massive migration. Among them, the drift path of *U. prolifera* in 2017 was the longest, which was approximately twice that of 2016 and 2018.

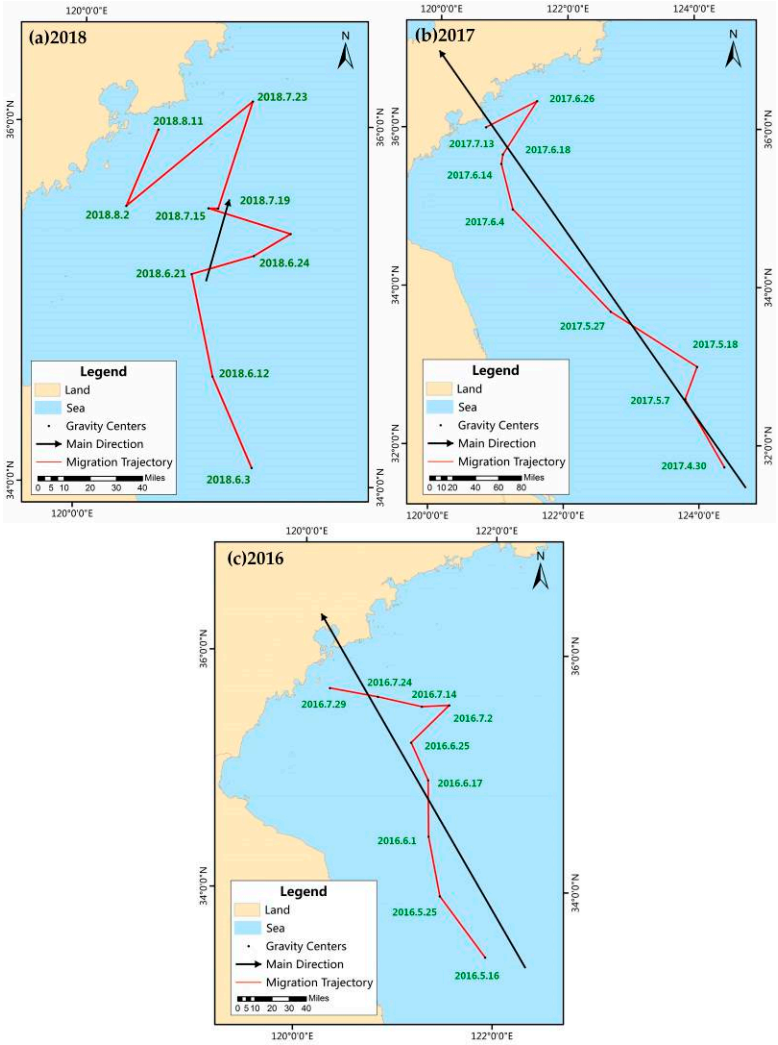

Figure 8. (**a**) Migration trajectory of the average barycenter in 2018. (**b**) Migration trajectory of the average barycenter in 2017. (**c**) Migration trajectory of the average barycenter in 2016. The direction of the black arrow in three graphs indicates the main direction of the path, and the length of the line represents the path length and the consistency of the subpaths, to some extent. Generally speaking, the longer the migration path is, the more consistent the direction trend of the subpaths is, and the longer the length of the main direction line is.

Over these three years, the rate of gradual northward migration in the north–south direction was remarkable, and the span in latitude was 2.1° in 2018, 4.6° in 2017 and 2.2° in 2016. Among them, the rotation of the drift path in the north–south direction only happened once in 2018 and 2017, severally. For most other time periods, the gravity centers kept moving north. Compared with the north—south direction, the range of movement in the east–west direction was smaller in 2016 and 2018, the span of movement was 1.6° and 1.13°, respectively. However, the longitude span was still relatively large, at about 3.6° in 2017. In 2018, the changes in the east–west direction fluctuated greatly, and there was no obvious regularity. Different from 2018, the movement in the east–west direction of 2016 and 2017 was significant—gradually moving westward, with only a small rotation phenomenon once or twice. Moreover, the starting point and the ending point of the trajectory were the westernmost position and the easternmost positions, correspondingly.

3.4. Morphological Characteristics of U. prolifera Distribution

3.4.1. Directionality

The SDE can be used to show the directional characteristics of the distribution of coverage points of *U. prolifera*. Figure 9 shows the SDE corresponding to different dates in 2018. Also, the SDE of *U. prolifera* in 2017 and 2016 can be seen in Figure 10. Because the direction angle and the oblateness of the ellipse are the two important parameters in this study, Figure 11 shows the variation curve of the standard deviation ellipse oblateness, and Figure 12 displays the directional angle of the ellipse of these three years.

The coverage of *U. prolifera* in different shapes was simplified to the SDE. The parameters of SDE can reflect the morphological characteristics of the coverage of the *U. prolifera* margin to some extent. Overall, there were large differences in the ellipse shape over different periods, both in direction and in oblateness. The larger the oblateness, the more directional the object distribution, and thus, more attention must be paid to the time node at which the oblateness shows an upward jump.

As can be seen from Figure 11a, a sharp increase in oblateness occurred three times during the monitoring period in 2018. The first period was from June 3 to June 12, with an increase from 0.47 to 0.73. In the second period, from July 19 to July 23, the ratio increased from 0.45 to 0.66. The third period was from August 2 (0.65) to August 11 (0.85). Among these periods, the oblateness reached a maximum on August 11, when directionality was significant. Figure 12a also shows that the elliptical direction rotated clockwise with the passage of time, where two large angles of rotation occurred, and the time of these angles coincided with the first two periods, with a sudden increase in oblateness.

Two sudden increases in oblateness can be easily founded in 2017 (Figure 11b) during two continuous periods, June 18 (0.47) to 26 (0.67) and June 26 to July 13 (0.88). However, there was no consistent pattern of changes in the SDE direction angle in 2017, and three mutations occurred. The first period was from April 30 to May 7, the second was from June 4 to 14, and the third was from June 14 to 18. Among them, the change in third period was enormous, reaching 115°.

In 2016, the flatness of the SDE slightly fluctuated, but it was at a relatively small level most of the time, except for the period from July 24 to 29, the flattening rate increased from 0.23 to 0.82. The direction angle of the ellipse appeared over three periods of significant change. From May 25 to June 17, the direction angle continuously rotated clockwise. The second mutation occurred in July 2 to July 14, and there was a large turn in the direction angle. Thereafter, the angular rotation direction was reversed prodigiously, reaching 132.1°.

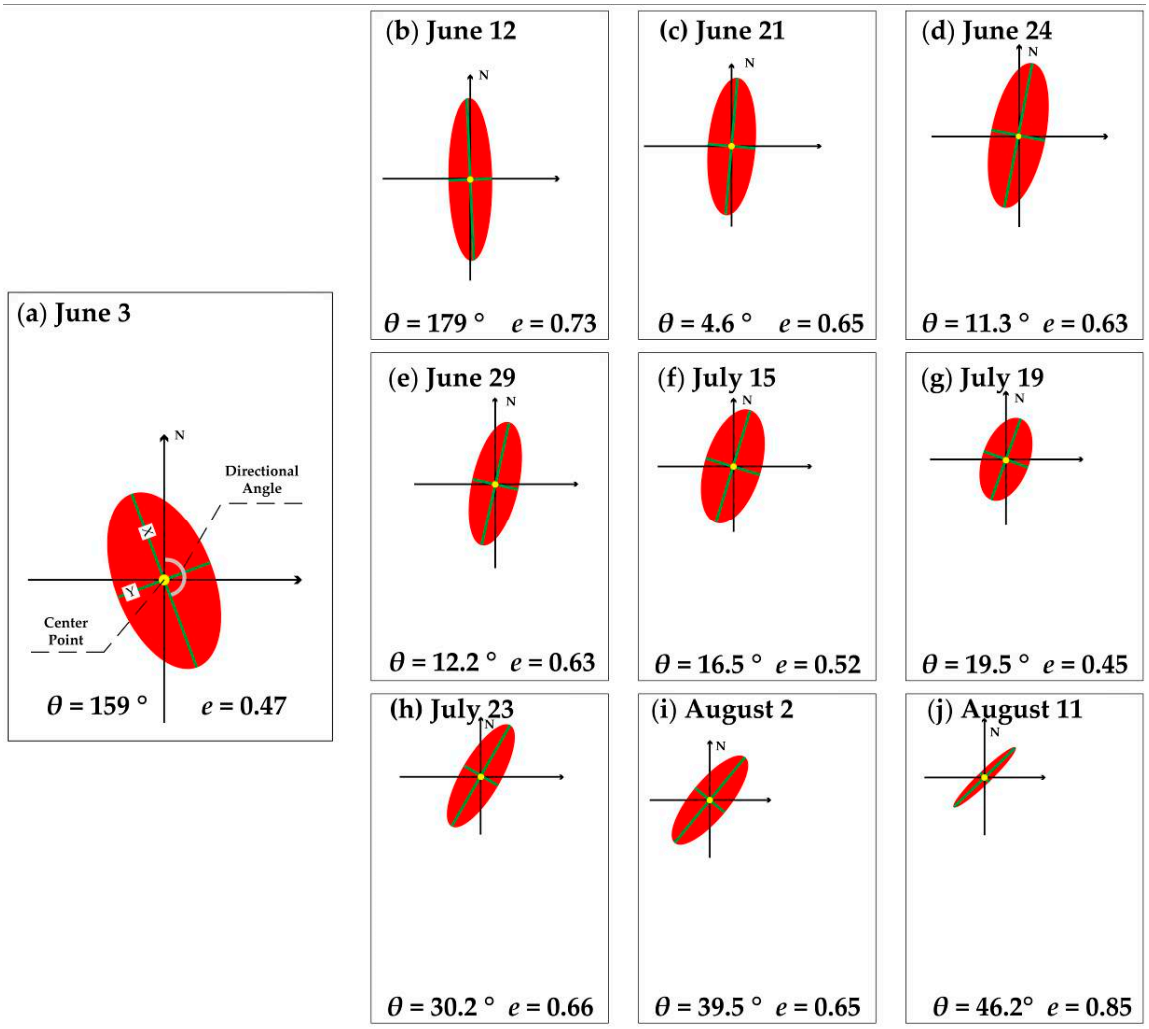

Figure 9. Standard deviation ellipse of the coverage area of *U. prolifera* in 2018. The first standard deviation ellipse was used in this paper, containing the data with a ratio of 68% (the proportion of data contained does not affect the values of two key indicators). (**a**) The SDE on June 3. (**b**) The SDE on June 12. (**c**) The SDE on June 21. (**d**) The SDE on June 24. (**e**) The SDE on June 29. (**f**) The SDE on July 15. (**g**) The SDE on July 19. (**h**) The SDE on July 23. (**i**) The SDE on August 2. (**j**) The SDE on August 11. Four parameters of the standard deviation ellipse are marked in (**a**). The yellow round dot is the elliptical center point, and the two green lines passing through the center point and perpendicular to each other are the X-axis and Y-axis, respectively. The angle between the north direction and the long axis is the directional angle, which is represented by an orange arc in the diagram. The annotation of these parameters is omitted from other subgraphs. The direction and oblateness of the ellipse are indicated at the bottom of each subgraph. θ represents the direction angle, whereas e is the oblateness.

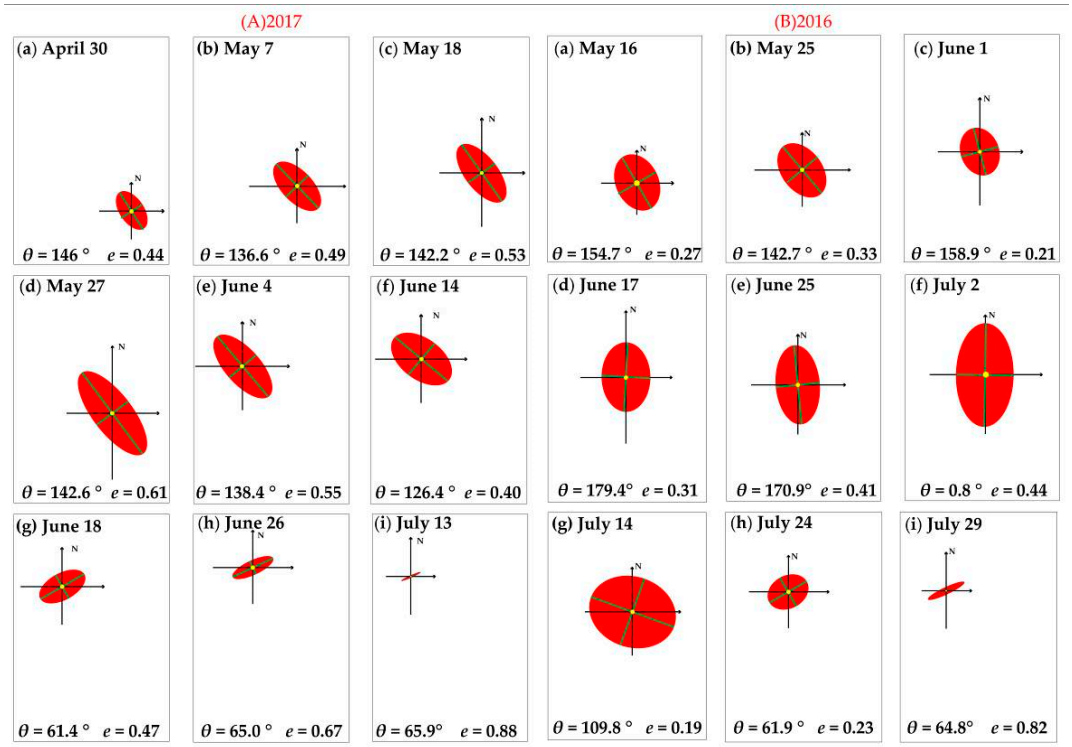

Figure 10. (**A**) Standard deviation ellipse of the coverage area of *U. prolifera* in 2017: (**a**) The SDE on April 30; (**b**) The SDE on May 7; (**c**) The SDE on May 18; (**d**) The SDE on May 27; (**e**) The SDE on June 4; (**f**) The SDE on June 14; (**g**) The SDE on June 18; (**h**) The SDE on June 26; (**i**) The SDE on July 13. (**B**) Standard deviation ellipse of the coverage area of *U. prolifera* in 2016: (**a**) The SDE on May 16; (**b**) The SDE on May 25; (**c**) The SDE on June 1; (**d**) The SDE on June 17; (**e**) The SDE on June 25; (**f**) The SDE on July 2; (**g**) The SDE on July 14; (**h**) The SDE on July 24; (**i**) The SDE on July 29.

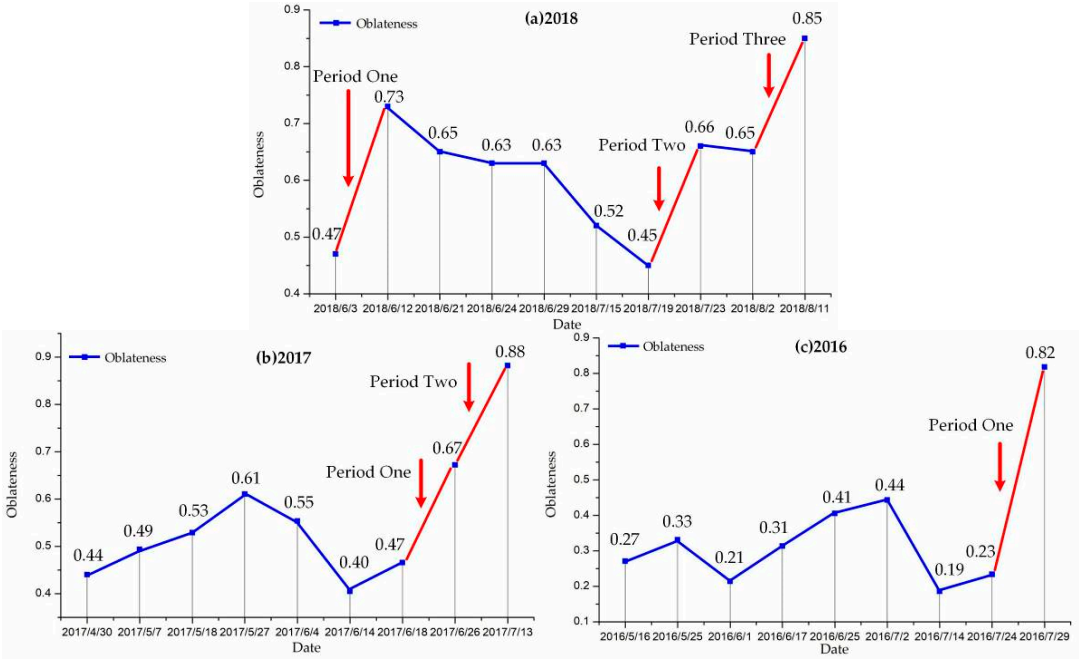

Figure 11. (**a**) Line chart of changes in oblateness in 2018. (**b**) Line chart of changes in oblateness in 2017. (**c**) Line chart of changes in oblateness in 2016. The horizontal coordinate is the date, and the vertical coordinate is the oblateness. The specific value of each date is marked above the broken line. The red segments in the figure indicate the periods when oblateness increased dramatically.

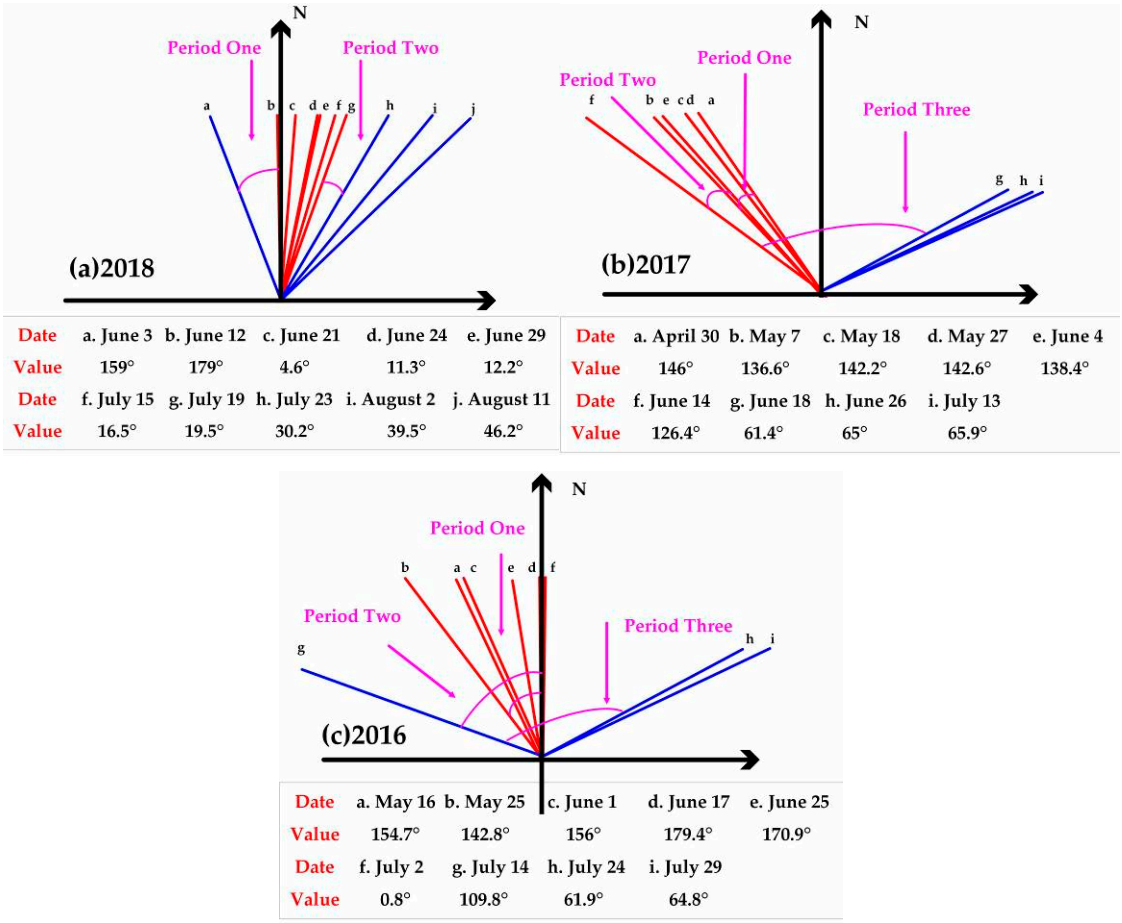

Figure 12. (**a**) Direction angle variation over time in 2018. (**b**) Direction angle variation over time in 2017. (**c**) Direction angle variation over time in 2016. The direction of the straight line (a, b, c, etc.) indicates the direction of the standard deviation ellipse on the corresponding date. Dates and values are marked on the right side of the figure. The vertical axis of the coordinate system is the north direction. Red and blue lines are used to highlight the process of abrupt angle changes, which are represented in the figure by magenta arcs.

3.4.2. Regularity

The perimeter area ratio is the ratio between the perimeter and the distribution area of *U. prolifera*, which is used to evaluate the regularity of the shape of the distribution range. To determine the variation in the perimeter area ratio, it was combined with the distribution area in Figure 13. The regularity of the two broken lines was very obvious and has the characteristics of trading off and taking turns in most periods.

In 2018, as time went by, the perimeter area ratio first decreased and then increased, whereas the area of influence rose first, and then declined. The pattern was the same for the most time of the other years. What called for special attention was that there was abnormal phenomena both in 2016 and 2017, and the time node was June 25 and May 18 separately, when the distribution area of *U. prolifera* reached maximum of the year. Over these two days, although the distribution area reached a tremendous value, the distribution boundary of *U. prolifera* was still irregular. In summary, in the vast majority of cases, compared with the distribution area, on days when the distribution area was smaller, the perimeter was longer.

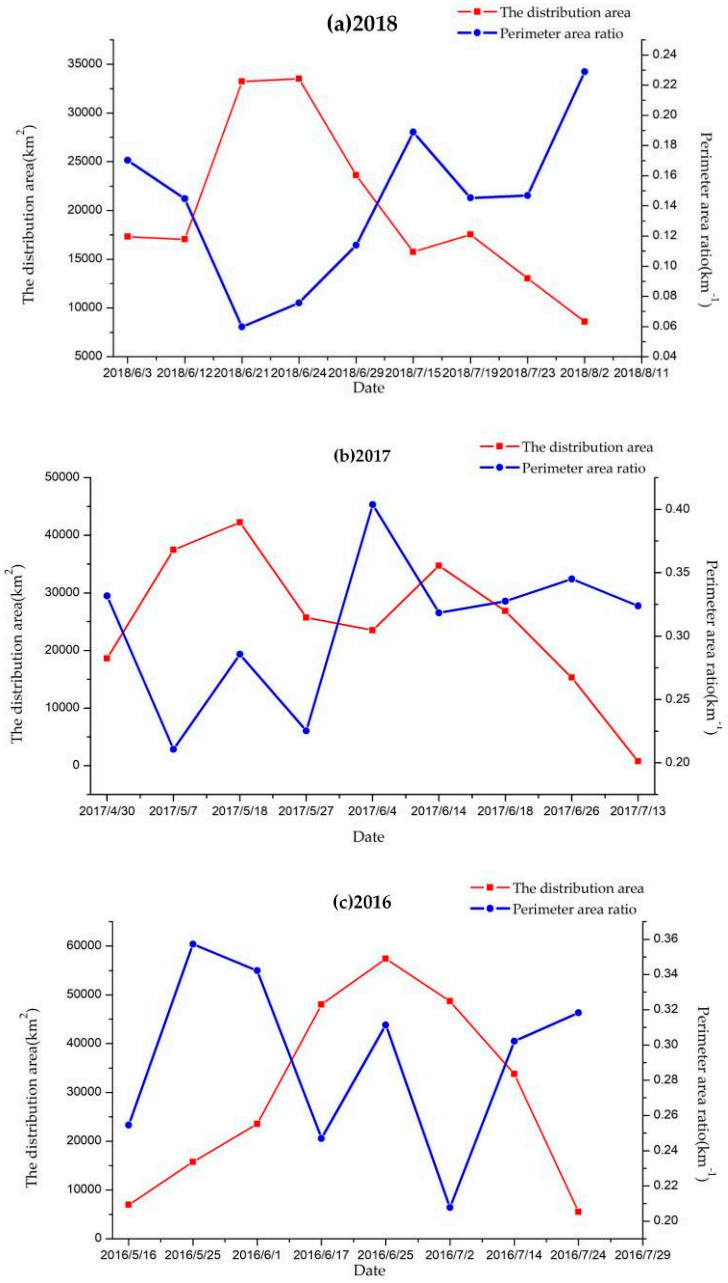

Figure 13. (**a**) Distribution area and perimeter ratio in 2018 are shown in the diagram as two broken lines. The transverse coordinates represent the time series. The left vertical coordinate is the distribution area, and the right vertical coordinate is the ratio of the perimeter to area. (**b**) Distribution area and perimeter ratio in 2017. (**c**) Distribution area and perimeter ratio in 2016.

4. Discussion

4.1. Spatiotemporal Features of U. prolifera

The spatiotemporal features of *U. prolifera* were compared from three viewpoints: the drift path, the overall situation, and the growth stages. First of all, this study found that the origination and the drift path of *U. prolifera* in 2016 and 2018 were still consistent with previous years. A large number of studies have shown that the green tides originate along the Jiangsu coast [30–33], which was first proposed by Liu et al. [2]. According to the growth of *U. prolifera* discovered for the first time on June 3 in 2018 (Figure 4a), the scale was still small, and growth was mainly distributed along the coastline of Jiangsu Province. However, because of the poor quality of MODIS images due to meteorological factors

in this year, it was impossible to judge the exact starting position and time of *U. prolifera*. Fortunately, the initial time that *U. prolifera* was found in 2016 was May 15, with a smaller distribution area and a similar position as in 2018 (Figure 5a). This discovery may help with speculation on the origination of *U. prolifera* in 2018. In terms of source tracing, unlike other years, 2017 presented a double-source phenomenon. On April 30 (Figure 6a), the *U. prolifera* was firstly discovered in the southeast corner of the Yellow Sea. On May 18 (Figure 6c), *U. prolifera* was founded near Jiangsu Province. Since the location span was very large, the time interval was short, and since then the growth of enteromorpha shown an obvious characteristic of rapid outbreak of one end and rapid disappearance of the other end, two different sources may be considered. Based on the analysis above, the hypothesis that Subei Shoal was the source of phytoplankton was confirmed again, though it was probably not the only source. Earlier investigations also indicated that the free-floating green tides in the Yellow Sea drifted to the southern coast of Shandong Province from June to August [10,16]. From 2016 to 2018, the floating angle has maintained a trend of gradual northward drift, accompanied by one or more north-to-south detours and finally drifted and died out near the vicinity of Qingdao.

Secondly, the overall situation of green tide events in 2016–2018 remained serious. Wu et al. [34] stated that from 2008 to 2012, the areas in 2008 and 2009 were obviously larger than in other years, with a maximum coverage area of 3451.19 km^2 and 2767 km^2 and an affected area of 23,475 km^2 and 26,234 km^2 in 2008 and 2009 respectively. From 2010 to 2012, the area was greatly reduced and relatively stable. However, Yang et al. [35] claimed that the maximum distribution area of green tide was increasing year by year from 2011 to 2016. During the three years 2016–2018 in this study, the maximum distribution and coverage area were 57,384 km^2 and 2906 km^2 in 2016. In the following two years, the distribution and coverage area relatively decreased, but still lead to a tremendous influenced marine area.

Normally, the development of macroalgal blooms in the Yellow Sea goes through five major stages: appearance, development, outbreak, decline (management), and disappearance [36]. From an interannual perspective, the five stages occur at different time periods in different years. Generally speaking, the earliest time of emergence was between the end of April and the beginning of May [31], with a relatively small coverage area and taking the form of algae filaments floating on the sea surface. In mid- to late May, as temperature, nutrient concentration, and other factors increased, the green tide continuously expanded. After the outbreak period in June and July, some green tide landfall occurred. Following a decrease in the coverage and distribution areas, the extinction period occurred in August [34].

In 2016 (Figure 14c), the growth of *U. prolifera* conformed to five growth stages, which appeared in mid-May, after a period of development, broke out in June. Since peaking on June 25, it declined rapidly and disappeared in late July. In contrast, the growth rules of *U. prolifera* in 2017 were quite different. In contrast, the growth rules of *U. prolifera* in 2017 (Figure 14b) were quite different, where two peaks occurred. From the end of April to the end of June, the scale of the floating angle was maintained at a relatively large level. The distribution area expended first, with a maximum occurring on May 18, and then it decreased until early June. In the middle of June, *U. prolifera* increased again and the coverage area reached the largest value of this year. After that, it shrunk quickly and almost died out in mid-July. In 2018 (Figure 14a), the variation in distribution area was almost consistent with previous years. Before June 3, the growth of *U. prolifera* was stable at the development stage. The outbreak began in mid-June, reached its peak on June 24, and then gradually decreased. It is worth noting that the coverage area change was governed by a different law. Between June 3 and 12, when the distribution area was stable, the coverage area doubled. After reaching a peak on June 24, the coverage area contracted sharply at first, and then remained on a plateau for nearly one month. This raises the problem of whether the coverage area was truly unchanged during this period. To answer this question, the migration trajectory was examined. From June 29 to August 2, when the macroalgal mat remained stable, there was a significant shift in the center of gravity of the coverage area. The interaction of the wind and tide fields most likely accounted for this dynamic change (this was discussed in Section 4.2).

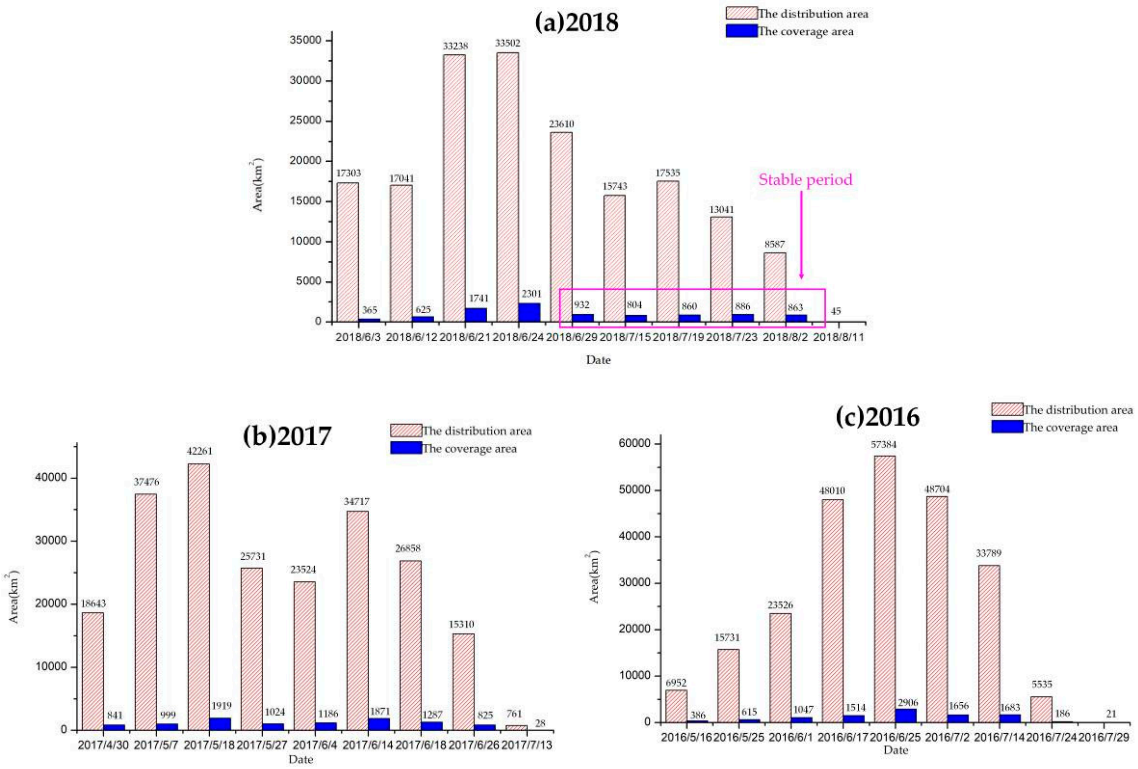

Figure 14. (**a**) Histogram of *U. prolifera* distribution and coverage area in 2018. The abscissa is the date, and the ordinate is the area in square kilometers. The stable period of the coverage area in 2018 is highlighted and marked by magenta boxes in the graph. (**b**) Histogram of *U. prolifera* distribution and coverage area in 2017. (**c**) Histogram of *U. prolifera* distribution and coverage area in 2016.

4.2. Influencing Factors of U. prolifera Migration

Generally, the changes in *U. prolifera* distribution are closely related to environmental factors. The growth of *U. prolifera* has a wide range of adaptation to seawater temperature, salinity, pH, and light intensity due to its undemanding requirements for marine environmental conditions [29]. Therefore, the main reasons for the migration were considered to be wind fields and ocean currents. Bao et al. [16] used a coastal ocean model to identify the processes that drive green algae drift. The results showed that, without wind, the research object displayed a tendency to move northward, but it was unable to move out of Subei Shoal. According to the drift path shown in Figure 8, a large area of algae was distributed outside Subei Shoal. Hence, this study focused on the relationship between *U. prolifera* migration and wind direction and speed.

To achieve the aim mentioned above, weekly average sea-surface wind (SSW) in the Yellow Sea during the monitoring periods in 2016–2018 was obtained from remote-sensing systems, (RSS) and is shown in Figure 15. Taking 2018 as an example, the detailed analysis is as follows: clearly, from early to mid-June, the northwest SSW gradually strengthened. During this period, the center of gravity of *U. prolifera* presented a constant northwesterly movement, with an increasing amplitude of variation. From June 17 to June 23, a circular wind in the clockwise direction appeared. In the occurrence area of *U. prolifera*, the wind direction changed from northwest to northeast, which led to a sudden change in the migration path of the center of gravity. Starting from June 21, the barycenter moved eastward, reaching its easternmost position of this year on June 29. However, after the beginning of July, the direction of the SSW reversed again, resulting in the center of gravity turning from east to west until mid-July. After that, the SSW remained constant from the northwest for a long time, and the wind speed was relatively stable. From the end of July to early August, the wind speed obviously weakened, and the direction deflected southward from the northwest. This explained the abnormal phenomenon of the southward barycenter movement. After August 4, *U. prolifera* moved northward

again as the SSW turned north, and the wind speed slightly increased. Based on the above analysis, the time nodes of SSW changed in direction and speed, and they were consistent, with changes in the *U. prolifera* trajectory during the whole monitoring period in 2018.

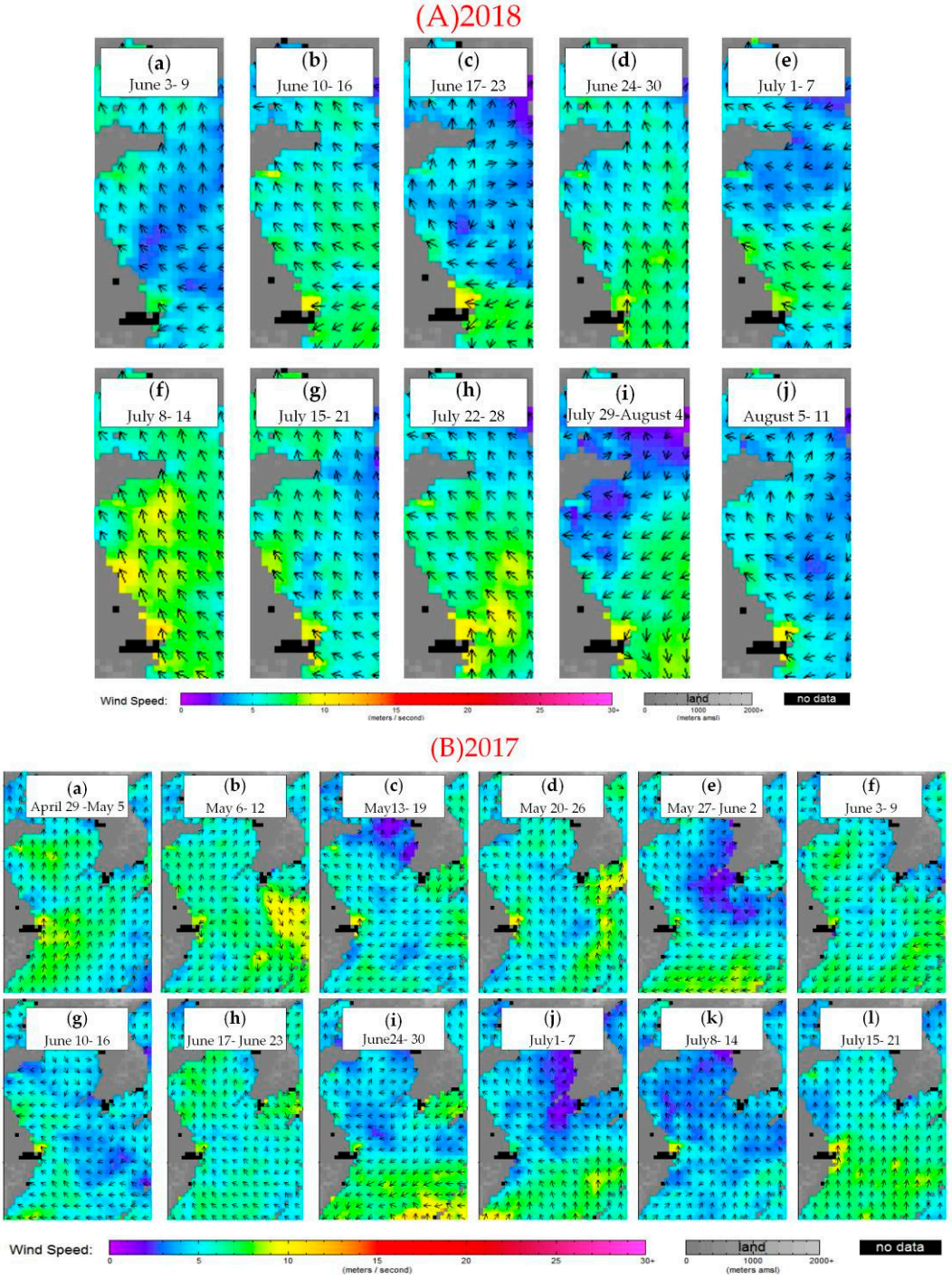

Figure 15. *Cont.*

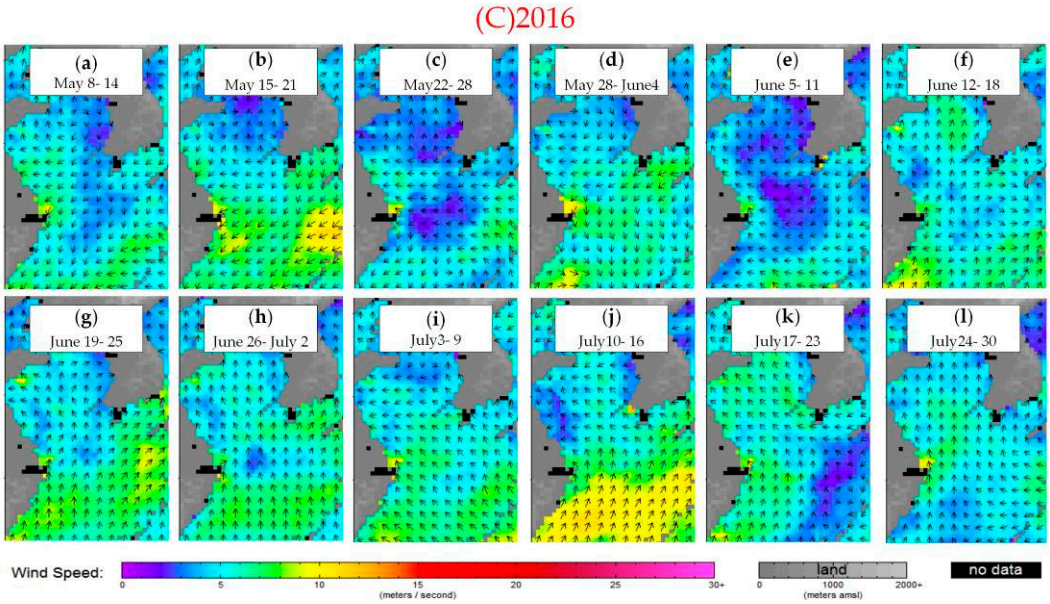

Figure 15. (**A**) Weekly average surface wind speed and direction from early June to mid-August in 2018. (**B**) Weekly average surface wind speed and direction from late April to July in 2017. (**C**) Weekly average surface wind speed and direction from early May to July in 2016. Dara was obtained from remote sensing systems (RSS), http://www.remss.com/. Remote Sensing Systems is supported by NASA, NOAA, and the NSF, offering research quality products of sea surface wind speed and direction and other products for use in research and climate study.

Most of time during 2017, the drift trajectory of *U.prolifera* basically coincided with the direction of the sea wind. It was worth noting that from May 18 to June 4, the movement of the trajectory to the west was tremendous. Especially from May 27 to June 4, in a short period of one week, the span of distance was extremely significant, regardless of the north–south or east–west directions. During this period, although the direction of the sea breeze was consistent, there was no sudden increase in wind speed. It was hard to imagine that such large-span movements were caused by the influence of the sea breeze. Therefore, based on the results of the *U. prolifera* growth situation analysis in Section 4.1, it could be speculated that two sources of *U. prolifera* existed in 2017, with great possibility of this being the case.

The tight relationship between the trajectory and the SSW also occurred in 2016. During the growth period of *U.prolifera*, from mid-May to the end of July, the wind direction of the SSW is basically northwest, which is consistent with the movement law of the trajectory. The period from June 25 to July 2 was only time period in the year where the track moved significantly eastwards. It then moved back from east to west during July 2–14, and it continued to move westward thereafter. From the corresponding SSW vector diagram, it can be found that in the first time period, the wind direction that originated in northwest direction was rotated upward toward the north, and the wind speed was also slightly reduced. In the second period, the wind returned to the original northwest direction, and then a southerly sea breeze with low wind speed appeared. This could also explain why the trajectory moved back to the west during this phase, and also moved slightly southward.

From a holistic point of view, the main direction of the SSW in the Yellow Sea in summer 2016–2018 was northwest, which was highly consistent with the main direction angles of the 2016 and 2017 tracks. In this study, the main direction of barycenter migration obtained by trajectory analysis in 2018 was 16° north by east, which was probably caused by the substantial eastward drift in late June. Furthermore, Figure 15 shows that the weekly average wind speed in the study area was low. The maximum wind speed was about 10 m/s, and the time period was quite short. For most of the time, the wind speed was 5 m/s to 7 m/s. Accordingly, a gentle SSW was enough to affect the distribution of *U. prolifera* and cause its migration.

4.3. Directionality Change and Sea Wind

Based on the change in SDE parameters, the influencing factors on algae distribution were further explored. It was also assumed that the sea breeze was the main influencing factor. During the three monitoring years in this study, the changes in oblateness and direction angle were quite different. The patterns in 2018 was easy to find, with three sharp increases in SDE oblateness (Figure 11a), and the direction being rotated clockwise with the passage of time (Figure 11b). Furthermore, the time periods where the two parameters changed greatly were important. In 2017 and 2016, the direction angle of SDE swung back and forth with no certain regularity, and there was a time period for where the angle rotated more than 100° clockwise in both years. Moreover, as in 2018, the flatness mutation occurred in the death stage of *U. prolifera*, with the maximum value of the oblateness occurring at the time when *U. prolifera* was close to extinction.

The analysis started from 2018. The three periods of oblateness change were in June 3 to 12, July 19 to 23, and August 2 to 11. In the first two time periods, the direction angle also changed greatly. Because the time span of the three periods was not long, the weekly averaged SSW data could not be used as a good basis. Therefore, a time interval of three days was used to determine whether the SSW changed suddenly, with the starting and ending date being taken as the search range. The results are shown in Figure 16. In these three periods, the wind direction changed, and the wind speed increased greatly.

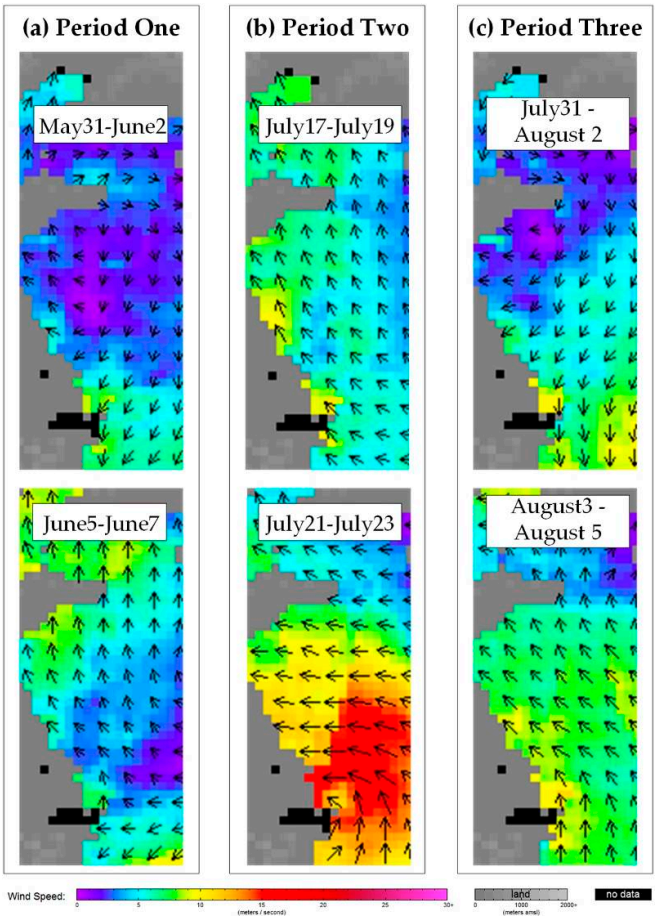

Figure 16. Three-day average surface wind speed and direction of three periods of oblateness change in 2018, obtained from RSS. In each specific period, the upper sub-graph represents the sea-surface wind (SSW) at the starting time, and the lower vector graph shows the changes in wind speed and direction within this period. (**a**) The change of SSW in period one. (**b**) The change of SSW in period two. (**c**) The change of SSW in period three.

Period one: From the end of May to the beginning of June, the SSW in the Yellow Sea was about 2 m/s, with inconsistent directions. However, the direction changed significantly heading north, and the speed increased two or three times. On June 3, the direction angle of the *U. prolifera* distribution was 21° north by west, approaching the coastline of Jiangsu Province. By comparison, on June 12, the north–south trend of the distribution was prominent. The direction angle was rotated strongly northward, and it almost reached the north direction. During this time period, the dramatic change in the shape of the distribution was closely related to the change in the SSW direction and the increase in wind speed.

Period two: From July 21 to 23, the wind speed suddenly increased to a maximum of 20 m/s, forming a huge windy area in the southern part of the Yellow Sea. On July 19 and 23, the distribution direction angle was 19.5° and 30.2° north by east, respectively. During this period, the wind direction was west and northwest, and the wind speed decreased with increasing latitude. The southern part of the distribution area was more strongly affected by SSW than the northern part, which may have accounted for the clockwise rotation of the direction angle.

Period three: At the beginning of August, the SSW was weak, at about 2 m/s, and the direction was westerly in the area where *U. prolifera* was distributed. From August 2 to 11, the wind speed increased significantly. The northwest wind directly pointed to the coastline of Shandong Province. In early August, *U. prolifera* was distributed in the sea area near Shandong Province. When the wind strengthened and the direction changed, *U. prolifera* was pushed further towards the shoreline. Until August 11, although the direction angle of the morphological distribution did not change significantly, and the directionality was significant, reaching its maximum value in 2018 and approaching the direction of the coastline of Shandong Province.

The oblateness changes in 2017 and 2016 were similar to the third period of 2018. At the same time as the mutation occurred, the oblateness reached the maximum value of the year. The situations in the disappeared stages of these three years are shown in Figure 4j, Figure 5i, and Figure 6i. It was obvious that *U. prolifera* was distributed along the coastline of Shandong, resulting in a prominence in directionality.

In 2017, a total of three sudden changes in the direction angle occurred. Similar to the analysis method in 2018, it took three days as a unit to find out whether there were great changes in the speed and direction of SSW in each period. Eventually, sudden changes in SSW were discovered during the first two periods, and the figures of SSW are shown in Figure 17. In these two periods, the direction angle was rotated counterclockwise. When the SSW changed with the same characteristic in the first period, it has shown an opposite trend in the second period. During that time, although the wind direction changed clockwise and the wind speed increased significantly, the direction angle of *U. prolifera* distribution still rotated counterclockwise. The abnormal phenomenon also occurred in the third period of time, during which the direction angle was reversed greatly, while no sudden change in wind speed or wind direction was observed. Based on the previous analysis of the *U. prolifera* growth trend in 2017, there were two sources in different periods in this year. Periods two and three, when the direction angle was abrupt, were exactly the time nodes for when one end of algae broke out and the other end declined.

In 2016, there were also three sudden changes in direction angles. Among them, the sea breeze changes in the first two periods are shown in Figure 18. During the first period, May 25 to June 17, the direction angle continued to rotate clockwise. Similar changes have taken place in the direction of the SSW. In the second period, July 2 to 14, in the area where the *U. prolifera* grew, the SSW originally pointed to the northern direction and the wind speed was relatively high. As time went by, the wind speed decreased and the direction pointed northwest. An anticlockwise wind circle was formed in the study area, which explained the change in the direction angle. Since the oblateness of the SDE indicates the significance of the distribution direction, the larger the value, the more significant the directivity. Therefore, when the oblateness value is very small, the distribution has no directional characteristics. In the third period of 2016, although the direction angle changed greatly, the change

was probably not caused by directional factors, for the reason that the oblateness values were very small throughout the period. The distribution situation of these two times nodes (Figure 6g, h) were compared, during which the large-area scattered angle died rapidly. This was probably the main reason for the change in direction angle.

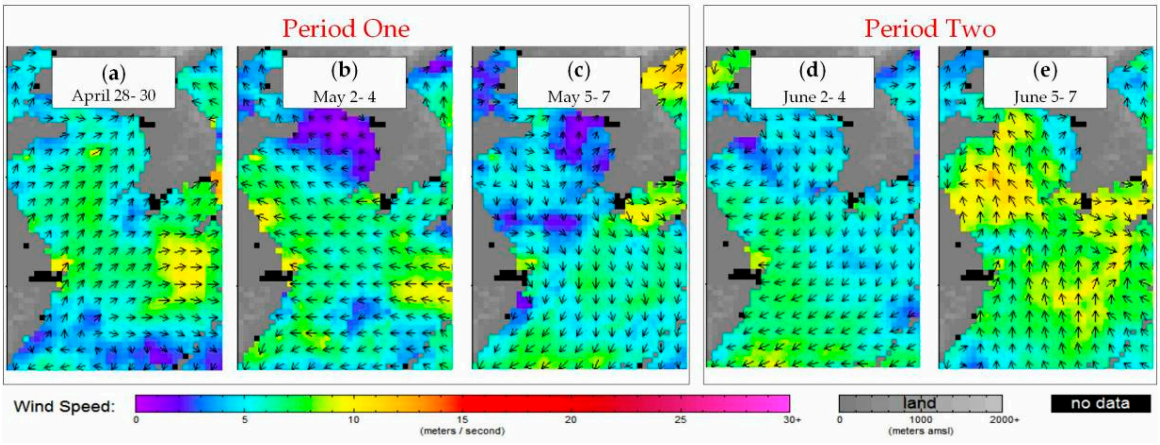

Figure 17. Three-day average surface wind speed and direction of oblateness change periods in 2017, obtained from RSS. (**a**–**c**) The change of SSW in period one. (**d**,**e**) The change of SSW in period two.

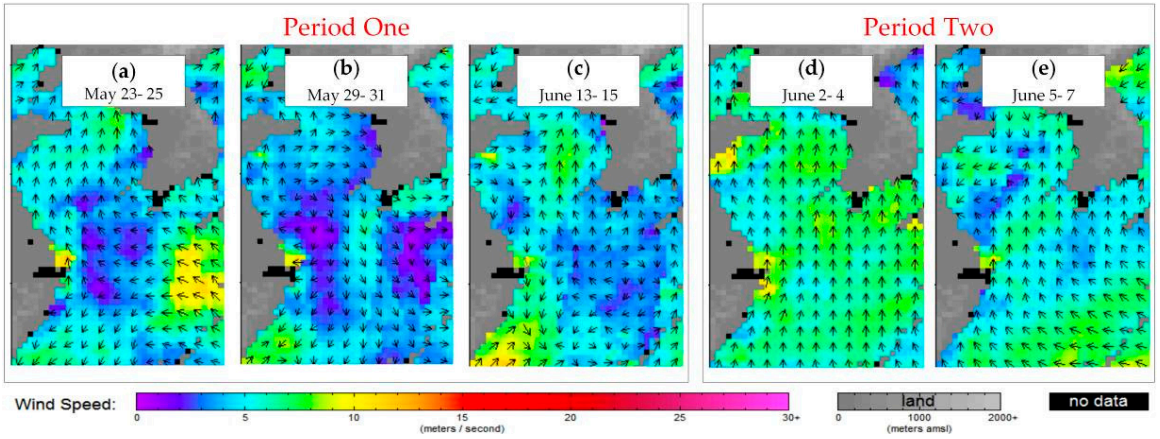

Figure 18. Three-day average surface wind speed and direction of oblateness change periods in 2016, obtained from RSS. (**a**–**c**) The change of SSW in period one. (**d**,**e**) The change of SSW in period two.

According to the analysis above, the change in SSW played a crucial role in influencing the distribution morphology of *U. prolifera*. The changes in direction angle caused by direction and speed of SSW were usually continuous, which could be confirmed by the three periods of 2018, the first period of 2017 and the first two periods of 2016. However, the sudden change of the SSW was not enough to cause the sharp reversal of the direction angle, which was found both in 2017 and 2016. The changes were most likely caused by the growth and decline of *U. prolifera* at different locations.

5. Conclusions

The world's largest macroalgal blooms have appeared in the Yellow Sea every summer since 2007, becoming a tricky, complicated, and repetitive issue for the marine environment. In this study, the NDVI index was used to extract information about the green tide from MODIS images during 2016–2018. Along with the overall morphology, the morphological characteristics of the *U. prolifera* distribution were analyzed. The conclusions were as follows:

- In recent years, the overall *U. prolifera* situation was still severe, with the largest distribution and coverage areas reaching 57,384 km^2 and 2906 km^2 on 25 June 2016. The growth pattern of *U. prolifera* has changed greatly in three years: in 2016, the growth of *U. prolifera* was basically in line with the five stages of previous years; in 2017, two peaks appeared in different time periods and different locations; in 2018, *U. prolifera* entered a month-long stable period, during which the center of gravity shifted significantly. In 2016, the largest scale occurred, and in 2017, the longest migration path was experienced. In contrast, the situation of *U. prolifera* in 2018 has been alleviated to a certain extent. Continuous monitoring of *U. prolifera* is conducive to obtaining a deep understanding of its growth cycle, grasping the changes in its development from year to year, and reassessing the severity of the green tide event.
- The total affected region was 163,162 km^2, of which the high-risk areas (with a probability of occurrence greater than 50%) were concentrated mainly in the small sea area near Qingdao. This finding provided a reference for manpower and resource allocation in preventing and treating this severe marine ecological problem.
- The trend of the migration track was basically consistent within these three years. *U. prolifera* drifted northwest, and finally died out in the sea area near Qingdao, Shandong Province. Representing the concentration point of the density, the center of gravity of *U. prolifera* goes hand in hand with its distribution. The migration of the barycenter is the basis of the growth prediction model, which is helpful in achieving the sub-regional and sub-period management of *U. prolifera*.
- The regularity of the boundary shape of the *U. prolifera* distribution showed an opposite change pattern to its scale variation. In most instances, the wider the distribution area, the more regular the shape and the denser were the algae, a finding that was beneficial for large-scale centralized management. On the contrary, when the distribution area was small, the shape of the boundary was variable, and collective salvage was not achievable.
- Changes in SSW in direction and speed were the main causes of *U. prolifera* migration, and they also accounted for changes in its distribution morphology. The relationship between SSW and the morphology parameters was conducive to optimizing and improving the *U. prolifera* prediction model. In addition to predicting the occurrence position of the green tide based on its center of gravity drift path, the distribution, direction, and scale of macroalgae blooms were further specified by using morphological parameters.

Monitoring *U. prolifera* development should be an ongoing project. Although the findings presented here can be explained by the SSW, they are preliminary in nature. Quantitative analysis of the correlation between SSW, *U. prolifera* drift, and morphological changes, leading to early warnings and the prediction of green tide events, will become the focus of future research.

Author Contributions: Conceptualization, Y.W., Y.C. and Z.F.; methodology, Y.W. and Z.F.; validation, Y.C., X.C., J.L. and X.S.; formal analysis, Y.C. and Y.W.; investigation, X.S.; writing—original draft preparation, Y.W.; writing—review and editing, Y.C. and Z.F.; visualization, Y.W.

Funding: The research was supported in part by National key R&D plan, grant number 2017YFC1405302; National Natural Science Foundation of China, Grants 41771473 and 41231171; and the Fundamental Research Funds for the Central Universities.

Conflicts of Interest: The authors declare no conflict of interest.

References

1. Liu, D.Y.; Keesing, J.K.; He, P.M.; Wang, Z.L.; Shi, Y.J.; Wang, Y.J. The world's largest microalgae bloom in the Yellow Sea, China: Formation and implications. *Estuar. Coast. Shelf Sci.* **2013**, *129*, 2–10. [CrossRef]
2. Liu, D.Y.; Keesing, J.K.; Xing, Q.G.; Shi, P. World's largest marcoalgal bloom caused by expansion of seaweed aquaculture in China. *Mar. Pollut. Bull.* **2009**, *58*, 888–895. [CrossRef] [PubMed]

3. Wang, C.; Yu, R.C.; Zhou, M.J. Effects of the decomposing green macroalga *Ulva (Enteromorpha) prolifera* on the growth of four red-tide species. *Harmful Algae* **2012**, *16*, 12–19. [CrossRef]
4. Zhang, J.H.; Huo, Y.Z.; Zhang, Z.L.; Yu, K.F.; He, Q.; Zhang, L.H.; Yang, L.L.; Xu, R.; He, P.M. Variations of morphology and photosynthetic performances of *Ulva prolifera* during the whole green tide blooming process in the Yellow Sea. *Mar. Environ. Res.* **2013**, *92*, 35–42. [CrossRef]
5. Li, L.; Xing, Q.; Yu, D.; Zhang, J. Assessment of the impacts from the world's largest floating macroalgae blooms on the water clarity at the west Yellow Sea using MODIS data (2002–2016). *IEEE J. Sel. Top. Appl. Earth Obs. Remote Sens.* **2018**, *11*, 1397–1402. [CrossRef]
6. Jiang, P.; Wang, J.F.; Cui, Y.L.; Li, Y.X.; Lin, H.Z.; Qin, S. Molecular phylogenetic analysis of attached Ulvaceae species and free-floating Enteromorpha from Qingdao coasts in 2007. *Chin. J. Oceanol. Limnol.* **2008**, *26*, 276–279. [CrossRef]
7. Ye, N.H.; Zhang, X.W.; Mao, Y.Z.; Liang, C.W.; Xu, D.; Zou, J.; Zhuang, Z.M.; Wang, Q.Y. "Green tides" are overwhelming the coastline of our blue planet: Taking the world's largest example. *Ecol. Res.* **2011**, *26*, 477–485. [CrossRef]
8. Zhao, J.; Jiang, P.; Liu, Z.Y.; Wei, W.; Lin, H.Z.; Li, F.C.; Wang, J.F.; Qin, S. The Yellow Sea green tides from 2007 to 2011 were dominated by one species–Ulva (Enteromorpha) prolifera. *Chin. Sci. Bull.* **2013**, *58*, 2298–2302. [CrossRef]
9. Hu, C.; He, M.X. Origin and offshore extent of floating algae in Olympic sailing area. *Eos Trans. AGU* **2008**, *89*, 302–303. [CrossRef]
10. Xing, Q.; Loisel, H.; Schmitt, F.; Shi, P.; Liu, D.; Keesing, J. Detection of the green tide at the Yellow Sea and tracking its wind-forced drifting by remote sensing. *Geophys. Res. Abstr. EGU Gen. Assem.* **2009**, *11*, EGU2009-577.
11. Qi, L.; Hu, C.; Xing, Q.; Shang, S. Long-term trend of *Ulva prolifera* blooms in the western Yellow Sea. *Harmful Algae* **2016**, *58*, 35–44. [CrossRef] [PubMed]
12. Hu, C.; Li, D.; Chen, C.; Ge, J.; Muller-Karger, F.E.; Liu, J.; Yu, F.; He, M. On the recurrent *Ulva Prolifera* blooms in the Yellow Sea and East China Sea. *J. Geophys. Res.* **2010**, *115*. [CrossRef]
13. Xing, Q.; Zheng, X.; Shi, P.; Hao, J.; Yu, D.; Liang, S.; Liu, D.; Zhang, Y. Monitoring "Green Tide" in the Yellow Sea and the East China Sea using multi-temporal and multi-source remote sensing images. *Spectrosc. Spectr. Anal.* **2011**, *31*, 1644–1647. (In Chinese)
14. Xing, Q.G.; Hu, C.M.; Tang, D.L.; Tian, L.Q.; Tang, S.L.; Wang, X.H.; Lou, M.J.; Gao, X.L. World's Largest Macroalgal Blooms Altered Phytoplankton Biomass in Summer in the Yellow Sea: Satellite Observations. *Remote Sens.* **2015**, *7*, 12297–12313. [CrossRef]
15. Xu, Q.; Zhang, H.; Ju, L.; Chen, M. Interannual variability of *Ulva prolifera* blooms in the Yellow Sea. *Remote Sens.* **2014**, *35*, 4099–4113. [CrossRef]
16. Bao, M.; Guan, W.B.; Yang, Y.; Cao, Z.Y.; Chen, Q. Drifting trajectories of green algae in the western Yellow Sea during the spring and summer of 2012. *Estuar. Coast. Shelf Sci.* **2015**, *163*, 9–16. [CrossRef]
17. Cui, T.; Zhang, J.; Sun, L.; Jia, Y.; Zhao, W.; Wang, Z.; Meng, J. Satellite monitoring of massive green macroalgae bloom (GMB): Imaging ability comparison of multi-source data and drifting velocity estimation. *Int. J. Remote Sens.* **2012**, *33*, 5513–5527. [CrossRef]
18. Son, Y.B.; Choi, B.J.; Kim, Y.H.; Park, Y.G. Tracing floating green algae blooms in the Yellow Sea and the East China Sea using GOCI satellite data and Lagrangian transport simulations. *Remote Sens. Environ.* **2015**, *156*, 21–33. [CrossRef]
19. Cui, T.W.; Liang, X.J.; Gong, J.L.; Tong, C.; Xiao, Y.F.; Liu, R.J.; Zhang, X.; Zhang, J. Assessing and refining the satellite-derived massive green macro-algal coverage in the Yellow Sea with high resolution images. *ISPRS J. Photogramm. Remote Sens.* **2018**, *144*, 315–324. [CrossRef]
20. Xing, Q.G.; Wu, L.L.; Tian, L.Q.; Cui, T.W.; Li, L.; Kong, F.Z.; Gao, X.L.; Wu, M.Q. Remote sensing of early-stage green tide in the Yellow Sea for floating macroalgae collecting campaign. *Mar. Pollut. Bull.* **2018**, *113*, 150–156. [CrossRef]
21. Xing, Q.; Hu, C. Mapping macroalgal blooms in the Yellow Sea and East China Sea using HJ-1 and Landsat data: Application of a virtual baseline reflectance height technique. *Remote Sens. Environ.* **2016**, *178*, 113–126. [CrossRef]

22. Yin, H.Y.; Liu, Y.J.; Chen, Q. An Elegant End-to-End Fully Convolutional Network (E3FCN) for Green Tide Detection Using MODIS Data. In Proceedings of the 2018 10th IAPR Workshop on Pattern Recognition in Remote Sensing (PRRS), Beijing, China, 19–20 August 2018; pp. 1–6. [CrossRef]
23. Lin, C.; Ning, X.; Su, J.; Lin, Y.; Xu, B. Environmental changes and the responses of the ecosystems of the Yellow Sea during 1976–2000. *J. Mar. Syst.* **2005**, *55*, 223–234. [CrossRef]
24. Level-1 and Atmosphere Archive & Distribution System Distributed Active Archive Center (LAADS DAAC). Available online: https://ladsweb.modaps.eosdis.nasa.gov/ (accessed on 15 June 2018).
25. Garcia, R.A.; Fearns, P.; Keesing, J.K.; Liu, D. Quantification of floating macroalgal blooms using the scaled algal index. *J. Geophys. Res. Oceans.* **2013**, *118*, 26–42. [CrossRef]
26. Jin, S.; Liu, Y.X.; Sun, C.; Wei, X.L.; Li, H.T.; Han, Z. A study of the environmental factors influencing the growth phases of *Ulva prolifera* in the southern Yellow Sea, China. *Mar. Pollut. Bull.* **2018**, *135*, 1016–1025. [CrossRef]
27. Zhao, Y.S.; Chen, D.M.; Li, X.M. *Analysis Principle and Method of Remote Sensing Applications*; Science Press: Beijing, China, 2003.
28. Rouse, J.W., Jr.; Haas, R.H.; Schell, J.A.; Deering, D.W. Monitoring Vegetation Systems in the Great Plainswith Erts. *NASA Spec. Publ.* **1974**, *351*, 309.
29. Lefever, D.W. Measuring geographic concentration by means of the standard deviational ellipse. *Am. J. Sociol.* **1926**, *32*, 88–94. [CrossRef]
30. Keesing, J.K.; Liu, D.Y.; Fearns, P.; Garcia, R. Inter- and intra-annual patterns of *Ulva prolifera* green tides in the Yellow Sea during 2007–2009, their origin and relationship to the expansion of coastal seaweed aquaculture in China. *Mar. Pollut. Bull.* **2011**, *62*, 1169–1182. [CrossRef]
31. Wang, Z.L.; Xiao, J.; Fan, S.L.; Li, Y.; Liu, X.Q.; Liu, D.Y. Who made the world's largest green tide in China?-an integrated study on the initiation and early development of the green tide in Yellow Sea. *Limnol. Oceanoger.* **2015**, *60*, 1105–1117. [CrossRef]
32. Li, H.M.; Zhang, Y.Y.; Tang, H.J.; Shi, X.Y.; Rivkin, R.B.; Legendre, L. Spatiotemporal variations of inorganic nutrients along the Jiangsu coast, China, and the occurrence of macroalgal booms (green tides) in the southern Yellow Sea. *Harmful Algae* **2017**, *63*, 164–172. [CrossRef]
33. Zhou, M.J.; Liu, D.Y.; Anderson, D.M.; Valiela, I. Introduction to the Special Issue on green tides in the Yellow Sea. *Estuar. Coast. Shelf Sci.* **2015**, *163*, 3–8. [CrossRef]
34. Wu, M.Q.; GUO, H.; Zhang, A.D.; Jia, L.L.; Xiao, L.X.; Wang, J.P. Research on the Characteristics of *Ulva Prolifera* in Shandong Peninsula During 2008-2012 Based on MODIS Data. *Spectrosc. Spectr. Anal.* **2014**, *35*, 1312–1318. (In Chinese)
35. Yang, J.; Zhang, S.; Liu, G.M. Variability analysis of the Green Tide based on satellite remote sensing monitoring data from 2011 to 2016 in the Yellow Sea. *Mar. Forecasts* **2017**, *34*, 56–61. (In Chinese)
36. Sun, X.; Wu, M.Q.; Xing, Q.G.; Song, X.D.; Zhao, D.H.; Han, Q.Q.; Zhang, G.Z. Spatio-temporal patterns of *Ulva prolifera* blooms and the corresponding influence on chlorophyll-a concentration in the Southern Yellow Sea, China. *Sci. Total Environ.* **2018**, *640–641*, 807–820. [CrossRef] [PubMed]